Watering the desert: Oasis hydroarchaeology, geochronology and functionality in Northern Arabia

Christopher Lüthgens,[1] [iD] Marta Luciani,[2,3] [iD]
Sabrina Prochazka,[1] [iD] Gustav Firla,[1] [iD] Philipp Hoelzmann,[4] [iD]
and Ahmed M Abualhassan[5]

Abstract

The phenomenon of very extended desert oases settlements, mega-sites featuring complex irrigation systems and monumental walls has long been observed in Northern Arabia. In the past, it has been linked to the settling down of nomadic components of the population and dated through archaeological material to the Late Bronze or Iron Ages (late second to mid-first millennium BCE). Since 2014 we have been investigating this development through the case study of the oasis of Qurayyah, a walled site of over 300 ha (Tabuk, NW Saudi Arabia). After mapping the geomorphological and hydroarchaeological layout of this ancient settlement, we established the age of key locations of the site through OSL and radiometric measurements from controlled stratigraphic excavations. We could thus confirm that a major – the largest so far documented in Arabia – flood protection and surface water harvesting system (SWHS) was developed already during the Early Bronze Age (2900–2600 calBCE) onto the relict late Pleistocene playa landscape. This sophisticated anthropogenic hydraulic infrastructure enabled the foundation of the river oasis and construction of the permanent walled settlement. Since different components of the SWHS erected on the site (dam, inlet, canals, weirs, outlet, etc.) resulted being synchronic, they are understood as functional elements of one and the same system. A test of the functionality of the identified SWHS for different rainfall scenarios has confirmed that the volume of its catchment's surface-water supply was sufficient for irrigation, productive and drinking needs of the large oasis since its Early Bronze Age creation.

Introduction and research area

Our research focuses on the archaeological site Qurayyah (28°79′N/36°02′E), situated in the province Tabuk, northwest Saudi Arabia (Figure 1a), bordered by the eastern foothills of the Hejaz, east of the Hisma range. It lies approximately 45 km south of the Jordan border and around 120 km east of the Red Sea at an altitude of about 800 m. a.s.l. (Luciani, 2019).

The surrounding landscape, known as the Tabuk Plain, consists of Palaeozoic sandstones and clays that represent continental to marginal marine and alluvial to fluvial environments (Alsharshan et al., 2001; Barth, 1976; Laboun, 2013). This plateau landscape's geomorphology is shaped by wadis (Figure 1), which deposited significant amounts of fine material of Quaternary age (Parr et al., 1970). Beneath the Tabuk Plain lies an essential artesian groundwater storage (Barth and Schliephake, 1998). This storage is one of today's most crucial groundwater aquifers, situated approximately 40–100 m below Tabuk (Al-Ahmadi, 2009). Today, this storage is exploited for irrigation purposes. The most common centre-pivot irrigation (Figure 1b) shapes the modern landscape (Vincent, 2008).

A new Saudi-Arabian-Austrian joint archaeological research project, led by the Saudi Commission for Tourism and National Heritage (now Heritage Commission, Ministry of Culture, Ahmed

M. Abualhassan) and the University of Vienna (Prof. Dr. Marta Luciani) started in 2014 for the first time to conduct systematic multi-disciplinary investigations on the site (Luciani, 2019; Luciani and Alsaud, 2018). While archaeological research has confirmed the presence of a human frequentation starting at least from the Pre-Pottery Neolithic B (PPNB) (Luciani and Alsaud, 2018), recent investigations have proven continuity of human settlement from

[1]Department of Civil Engineering and Natural Hazards, Institute of Applied Geology, University of Natural Resources and Life Sciences, Vienna, Austria
[2]Department of Prehistoric and Historical Archaeology, University of Vienna, Austria
[3]HEAS – Human Evolution and Archaeological Sciences, University of Vienna, Austria
[4]Department of Earth Sciences, Institute of Geographical Sciences, Freie Universität Berlin, Germany
[5]Heritage Commission of the Ministry of Culture, Saudi Arabia

Corresponding author:
Christopher Lüthgens, Department of Civil Engineering and Natural Hazards, Institute of Applied Geology, University of Natural Resources and Life Sciences, Vienna, Peter-Jordan-Str. 82, Vienna 1190, Austria.
Email: christopher.luethgens@boku.ac.at
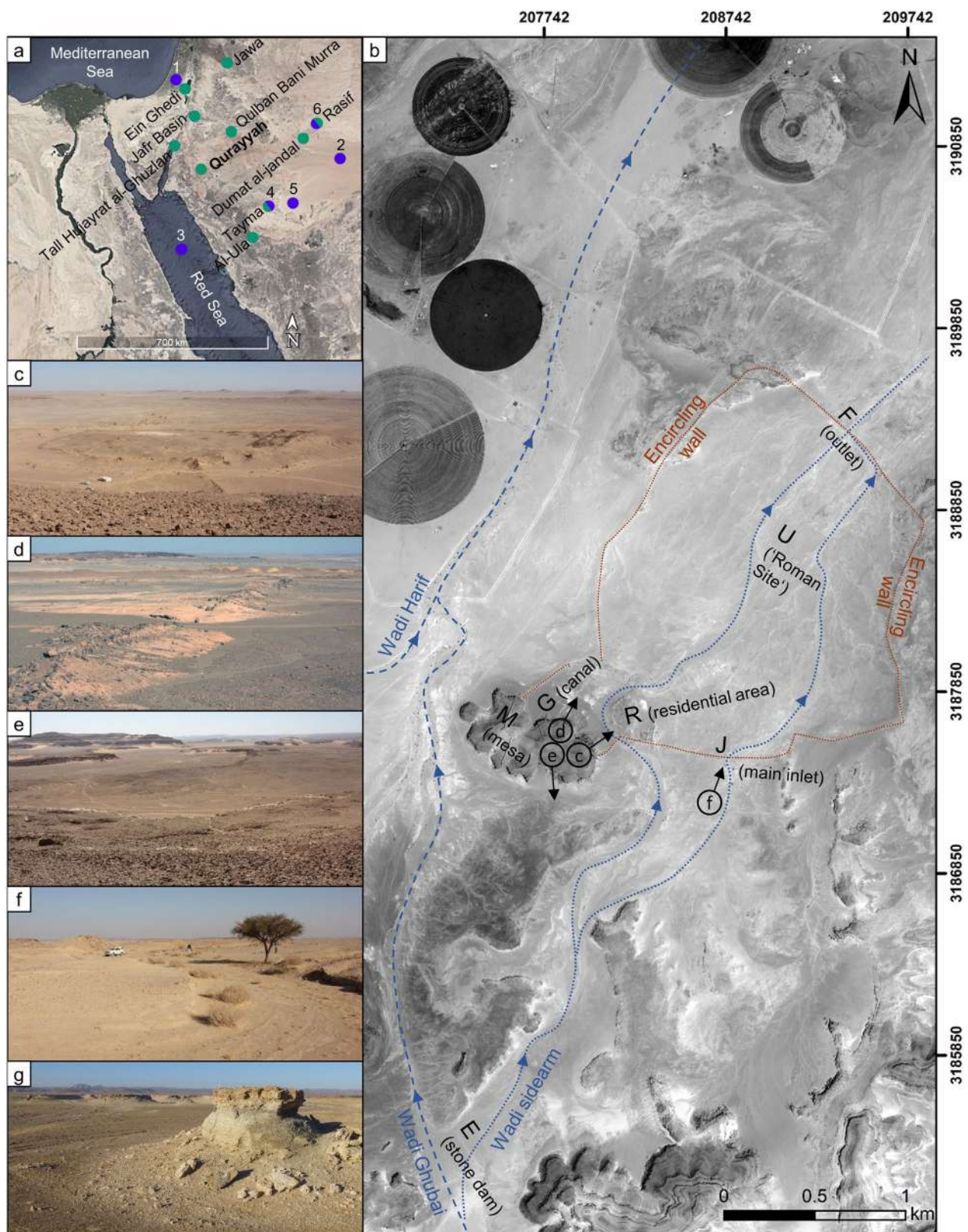
Figure 1. (a) Overview map showing the location of Qurayyah and other main oases (green dots) on the NW Arabian Peninsula, as well as important palaeoclimatic archives (numbered purple dots): 1. Soreq Cave, Israel (Bar-Matthews and Ayalon, 2011), 2. An Nafud, Saudi Arabia, (Whitney et al., 1983), 3. Shaban Deep basin, Red Sea (Arz et al., 2006), 4. Tayma, Saudi Arabia (Engel et al., 2012), 5. Alshabah, Saudi Arabia (Scerri et al., 2018), 6. Rasif, Saudi Arabia (Zielhofer et al., 2018); (b) Pansharpened GEOEYE satellite image with UTM coordinates (acquired on 15 September 2015, GEOEYE sensor Digital Globe, licenced to the University of Vienna) of Qurayyah and the surrounding area: Dashed lines indicate the main wadis (Ghubai and Harif), dotted lines mark the wadi sidearm leading to Qurayyah with arrows indicating the flow direction. A dotted line indicates the encircling settlement wall. Within this broader area, capital letters indicate the main research areas: E stone dam, F) outlet, G) water canal, J) main inlet, M) mesa with stone walls and semicircular stone tower, R) residential area and side inlet, U) water distribution canals and 'Roman site'; Subsets c-g show selected photos of the site, with corresponding letters in subset b showing the locations of the photos and respective arrows indicating the viewing direction, with the location of g not depicted on the map: (c) residential area and side inlet (Area R), (d) water canal (Area G), (e) wadi sidearm as seen from the mesa with Area E on the horizon, (f) main Inlet (Area J), (g) yardang in the wadi bed about 3 km NE and downstream of the main outlet at Area F; all photos by C. Lüthgens in 2017, except yardang in g taken by P. Hoelzmann in 2015.

the Early Bronze Age down to the Iron Age, the Nabatean, Roman and late Byzantine period (Luciani, 2019). One of the major research questions remains: establishing chronology and modalities of the formation of a permanent settlement in the oasis of Qurayyah, enclosed by a stone-and-mudbrick wall and including an extensive agricultural area with a surface water harvesting and irrigation system (Ingraham at al et al., 1981; Parr et al., 1970), which is possibly among the largest and earliest of the entire Arabian Peninsula (Masry, 1977). From its earliest phase (Early Bronze Age), we have 14C-dated macro-remains pointing to an established cultivation of olive groves (Luciani, 2021b). A continuous paleoclimate archive at Qurayyah is not available, but only discontinuous sedimentary records. Relevant palaeoclimatic reference sites are included in Figure 1a (for references please see figure caption), to provide a palaeoclimatic framework for the discussion of the results. Among these sites, the oasis of Tayma is the nearest site providing a continuous palaeoclimatic record based on the analysis of sabkha deposits (Engel et al., 2012; Neugebauer et al., 2022).

The urban-sized, ancient oasis settlement of Qurayyah is structured in two different units. In the southwest, a 50 m high, 1.2 km by 350 m inselberg (called the Rock Plateau, Figure 1b, Area M) features two long cross stonewalls with engaged and free-standing towers and several graves. Immediately to the northeast, at ground level, there extends a ca. 300 ha area encircled by an over 13 km long stone-and-mudbrick wall (Figure 1b).

This wide extension of the site includes both a circular-ogival, mudbrick-walled, smaller Residential Area (ca. 5 ha; Figure 1b Area R, Figure 1c) in the south and an ample layout of fields and channels throughout (ca. 275 ha; Figure 1b). A large hydraulic structure in the north dubbed 'Roman Site' was mapped by Parr et al. (1970) (Figure 1b Area U). An expanse of ca. 150 ha outside of the walled site displays similar fields partitioned by low-lying stone walls as visible inside the walled area. An additional similar terrain with stone partitions that may equally well belong to Qurayyah is located ca. 5 km SE of the site (Hüneburg et al., 2019). Thus, it potentially brings the entire agricultural area of the large walled settlement to ca. 600 ha. Not only such an extended district of irrigated fields but also the dry playa basin for the erection of the entire oasis settlement were made possible by the exceptional engineering feat of building a NW-SE, 350 m-long, stone dam 2 km upstream from the site and the agricultural fields themselves.

Settlement structure and geomorphology – identifying key sites for sampling: Defining Qurayyah's surface water harvesting system (SWHS)

Geomorphologically, (Figure 1a) the landscape is opening and very gently sloping to the northeast from a distinctive mesa, embossing the oasis. The quasi-plain on which the main settlement area of Qurayyah is located is hydrologically influenced by two cross-regional wadis, Wadi Harif in the west and Wadi Ghubai in the south, which form the most distinctive valley structures in the research area (Figure 1b). These wadis, dry riverbeds with episodic discharge, are the main routes capable of transporting water and sediments from the Hejaz's foothills to the Tabuk basin. The current wadi channels have a width of about 40–70 m and are incised into the several 100 m wide valley floors up to 3–4 m depth. Wadi Ghubai and Wadi Harif unite in the western vicinity of the oasis.

However, only Wadi Ghubai is directly connected to the settlement via a sidearm branching from the main wadi bed about 2.6 km south of Qurayyah (Figure 1b). This wadi sidearm's valley floor is typically between 150 and 300 m wide and characterised by a relief mainly shaped by fluvial processes. Once the sidearm reaches the distinctive mesa southwest of the settlement area, the valley widens to a quasi-planar area only partly surrounded by cuesta and mesa type elevations (Figure 1b). This quasi-plain has an approximate area of 7.3 km² and gently dips by less than a half degree (between the main inlet, Figure 1b, Area J, and the outlet, Figure 1b, Area F) to the northeast. Following this minimal gradient, runoff on the quasi-plain follows a general southwest to northeast direction. Although the surface morphology was significantly altered by human activity, it is still recognisable that the mainly fluvially shaped surface is intertwined with shallow, playa-like depressions.

During the field campaign in November 2018, it could be observed that after a short rainfall event, rainwater still accumulated in these drainless depressions. Such seasonally filled local depressions are called Qa'a and were described to occur in other oases on the Arabian Peninsula where they were used as open water storage (Al-Homoud et al., 1996; Gebel and Wellbrock, 2019; Meister et al., 2018b). Besides, minor sediment remobilisation was documented after rainfall events in 2018. These processes were most likely related to surface runoff from the local surrounding elevations. Flooding events originating from Wadi Ghubai were not documented in recent times, which may be related to the observed incision of the main wadi streams, causing a cut-off of the branching side-valley leading to Qurayyah. About 4 km to the NNE from the main outlet (Figure 1b, Area F) and after the confluence of Wadi Harif and Wadi Ghubai the landscape is characterised further downstream by the occurrence of yardang fields as shown in Figure 1g.

The settlement's Rock Plateau (mesa), dominating the southwest, consists of alternating layers of silt-, clay- and primary sandstone, interrupted by limestone veins (Parr et al., 1970; Wellbrock et al., 2018). Leaching processes in carbonate-rich layers likely developed a karstic system within the plateau, routing precipitation from the top of the plateau to its base, where fracture springs form at sedimentary boundaries. For a detailed geomorphological mapping of the area, we refer to Hüneburg et al. (2019).

Our initial study of the site's geomorphology (Hüneburg et al., 2019), including the walled area of the agricultural fields, indicated clearly that such a settlement could not have been established unless some control of surface water regimes was organised. In fact, we discovered a stone dam 2 km upstream from the settlement (Figure 1b, Area E) and we identified distinct openings in the settlement's walls, which functioned as inlets (Figure 1b, Area J and close to Area R) and outlet structures (Figure 1b, Area F). These basic hydrological structures embedded into the previously described geomorphological context, show close resemblance to the main elements of Arabian wadi farming techniques summarised by Reilly (2015) under the umbrella term *sayl* or floodwater-diversion agriculture, which is in general based on techniques for controlling and diverting surface runoff water from wadis to agricultural areas. This type of surface water harvesting system (SWHS) can clearly be differentiated from alternative watering techniques on mountain terraces or systems based on qanats and draw wells (Reilly, 2015).

In order to establish a chronology for this hydrological-anthropic system, we sampled sandy sediments for optically stimulated luminescence (OSL) dating in four key locations (chapter "Reliability and significance of luminescence ages"): the stone dam upstream of the site (Figure 1, Area E); the supposed inlet in the south (Figure 1, Area J) and in the north the outlet through the town wall (Figure 1, Area F) and finally one recognisable water canal inside the site (Figure 1b, Area G, Figure 1d). This data was then compared with the outcome of

Table 1. Basic data of luminescence samples and results from radionuclide analyses.

Area (cf. Figure 1)	Coordinates (decimal degrees, WGS 84)	Altitude (m)	Sample (lab code)	Sample (field code)	Depth (cm)[1]	^{238}U activity (Bq/kg)	^{232}Th activity (Bq/kg)	^{40}K activity (Bq/kg)
E (stone dam)	28.76191 (N) 36.00279 (E)	806	VLL-0267-L	QU.E.351.S.1	45	22.9 ± 1.7	26.4 ± 1.4	202 ± 12
			VLL-0268-L	QU.E.351.S.2	40	19.5 ± 1.5	22.3 ± 1.3	142 ± 9
			VLL-0269-L	QU.E.353.S.1	40	39.4 ± 2.6	42.8 ± 2.3	476 ± 29
			VLL-0270-L	QU.E.354.S.1	30	20.1 ± 1.5	23.4 ± 1.4	146 ± 9
			VLL-0271-L	QU.E.355.S.1	15	18.5 ± 1.5	22.3 ± 1.2	152 ± 9
			VLL-0316-L	QU.E.1001.S.15.L	10	44. 5 ± 3.0	52.4 ± 2.9	586 ± 35
			VLL-0317-L	QU.E.1002.S.15.L	10	48.8 ± 3.2	47.3 ± 2.6	526 ± 32
J (main inlet)	28.78178 (N) 36.01687 (E)	792	VLL-0279-L	QU.J.398.S.1	50	108.5 ± 6.6	42.7 ± 2.7	496 ± 30
			VLL-0280-L	QU.J.399.S.1	50	83.6 ± 5.1	40.7 ± 2.5	510 ± 31
			VLL-0281-L	QU.J.400.S.1	50	68.1 ± 4.4	33.3 ± 1.8	451 ± 27
			VLL-0319-L	QU.J.1004.S.1	50	30.6 ± 2.1	20.7 ± 1.2	229 ± 14
G (canal)	28.78393 (N) 36.00710 (E)	794	VLL-0275-L	QU.G.371.S.1	15	42.3 ± 3.0	56.2 ± 3.1	753 ± 45
			VLL-0276-L	QU.G.372.S.1	25	50.0 ± 3.0	53.9 ± 3.0	614 ± 37
			VLL-0277-L	QU.G.372.S.2	25	36.6 ± 2.6	52.5 ± 2.9	613 ± 37
			VLL-0278-L	QU.G.375.S.1	45	44.2 ± 3.1	63.6 ± 3.9	694 ± 42
F (outlet)	28.79833 (N) 36.02305 (E)	773	VLL-0272-L	QU.F.362.S.1	50	46.1 ± 3.0	25.6 ± 1.4	251 ± 15
			VLL-0273-L	QU.F.363.S.1	50	n/a[2]	n/a[2]	n/a[2]
			VLL-0274-L	QU.F.365.S.1	50	99.9 ± 6.3	49.1 ± 3.0	641 ± 29
			VLL-0318-L	QU.F.1003.S.1	50	79.9 ± 5.1	72.3 ± 4.2	617 ± 37
			VLL-0370-L	QU.F.1040.S1	50	95.9 ± 6.3	43.8 ± 2.5	537 ± 32
			VLL-0371-L	QU.F.1041.S2	50	96.4 ± 6.0	38.0 ± 2.4	795 ± 30

[1]For the samples from areas E and G, the values correspond to the sample depth below surface in vertical orientation. For the samples from areas J and F, however, it has to be taken into account, that these samples were taken from anthropogenic structures, so that an influence from cosmic rays penetrating also from the sides of the structures can not be ruled out completely. To reflect this, the depth values provided for samples from these areas represent an approximation of the distance of the samples from the structures' closest surfaces including the sides. For the exact positions of the samples in the outcrops, please see Figure 2.

[2]No suitable material for luminescence dating purposes could be extracted from sample VLL-0273-L, so consequently no measurements for radionuclide determination were conducted.

the radiometric measurements of organic remains found in controlled stratigraphic excavations (Luciani, 2019; chapter "Age crosscheck using radiocarbon dating"). We evaluated each dating method independently, because they determine different events in the past: OSL determines depositional ages of sediments, while radiocarbon dating of biogenic material determines the point in time when the incorporation of ^{14}C to the sampled material stopped – usually representing the death of an organism. However, comparing the results from the two different methodologies provides an invaluable crosscheck of our approach's validity.

In addition to these double chronological measurements, in order to verify the functionality of the entire system, we identified and mapped major hydraulic structures (chapter "Interpretation of the functionality of the investigated key structures") and conducted a plausibility check combining remote-sensing data and run-off calculations (chapter "Plausibility check of the SWHS").

# Establishing a numerical chronology

The lack of preserved organic material in the context of all but two of the key sites in a landscape today dominated by denudation processes minimises the chances of applying radiocarbon dating, which relies on organic material. Here, luminescence dating techniques come into play, enabling direct dating of minerogenic sediments. Luminescence dating techniques enable age determination ranging from years and decades to thousands and hundreds of thousands of years (Preusser et al., 2008; Rhodes, 2011; Wintle, 2008). A total of 21 samples (Table 1) for luminescence dating purposes were taken at the key sites described above in the part on

settlement structure and geomorphology (Figure 1). To better constrain the timing of human-made structures in this study, OSL dating techniques were applied to sediments under- and/or over-lying the structures, providing bracketing ages for the structure, or to materials incorporated in the structures, providing direct dating of building materials. Figure 2 shows the details of the sampled sections. Seven samples were taken at area E; four were taken at area J; four at area G, and six at area F (Figures 1 and 2). When sampling for luminescence dating purposes, it is essential to avoid sunlight exposure. Therefore, plastic or metal tubes with a length of 20 cm and a diameter between 5 and 7 cm were driven into newly opened and cleaned sediment sections. After sampling, both ends of the tubes were sealed with aluminium foil and black plastic. Additional samples from the direct surroundings of the OSL sampling spots were taken for radionuclide analysis. Details of the individual sampling locations are provided in Figure 2 and Table 1.

In general, the application of luminescence dating techniques enables the determination of depositional ages of sediments. It relies on the fact that quartz and feldspar minerals act as natural dosimeters. The equivalent dose D_e (total energy in Gy deposited in the crystals since the last zeroing of the luminescence signal) and the dose rate (total natural occurring radiation energy per time in Gy/a imparted on the minerals) must be known to calculate a sample's age. The general age equation is

$$age\,a = \frac{equivalent\,dose\,(Gy)}{dose\,rate\,(Gy\,/\,a)}$$

For details on luminescence dating in general, please see the following overview papers (Preusser et al., 2008; Rhodes, 2011;
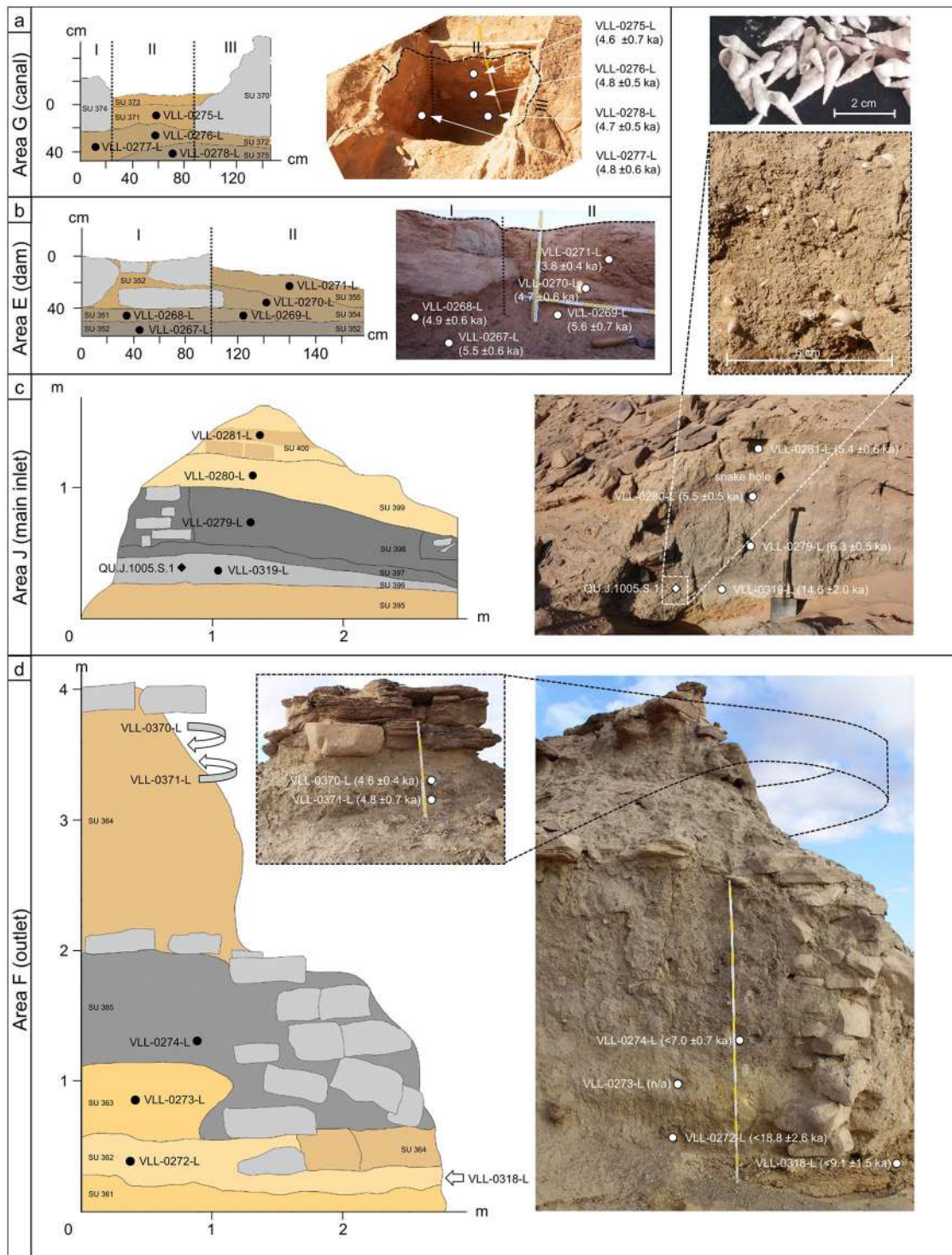
Figure 2. Detailed depiction of sampling sites showing sections' sketches with stratigraphic units (SU) and photos with sampling spots (black in the sketches and white in the photos) for dating samples. All ages are provided in ka. For ages in ka BCE please see Table 2. A detailed description of the stratigraphic units is provided in Supplemental Table S1. (a) Area G (canal): The dashed lines in the sketch (left) indicate ~90° angles in the investigated section, resulting in three section segments I, II and III (compare photo to the right). Please note that the walls of the canal are constructed using stones, the bottom of the canal however consists of sediments. (b) Area E (stone dam): The dashed line in the sketch (left) indicates a ~90° angle in the investigated section, resulting in two section segments I and II (compare photo to the right). Luminescence dating samples were taken from sediments deposited below and towards the side of the dam construction (unhewn stones and mud mortar, SU 352). (c) Area J (main inlet): The sketch (left) and photo (right) show an outcrop in the western wall of the inlet. Luminescence dating samples were taken from sediments below and within the construction, with the topmost stratigraphic unit (SU 400) consisting of silty mudbricks. Stratigraphic unit SU 396 contains snail shells (see detail enlargements above the outcrop photo), which were sampled for radiocarbon dating (sample QU.J.1005.S.1). (d) Area F (outlet): The sketch (left) and photos (right) show the outcrop in the NW wall of the outlet. The lowermost sample VLL-0318-L was taken from fine sandy sediments (SU 362) above the bedrock. The three samples above were taken from the material representing the main volume of the base of the outlet wall, whereas the two topmost samples were taken from material sandwiched between anthropogenic layers of unhewn stones (see detail enlargement showing the back of the outcrop as indicated in the photo to the right). All photos taken by M. Luciani (a/b/c in 2016, and d in 2018 apart from detail enlargements of snail shells in b taken by C. Lüthgens in 2017).

Wintle, 2008); for radiocarbon dating, detailed information is available from the following resources (Hajdas, 2008; Hajdas et al., 2021; Taylor and Bar-Yosef, 2014).

Experimental setup for OSL dating

The sample preparation was conducted using a standardised preparation technique (Lüthgens et al., 2017; Rades et al., 2018) in the Vienna Laboratory for Luminescence dating (VLL) under subdued red-light conditions.

Quartz was the mineral of choice for all measurements conducted in this study. Because it is known to bleach faster than feldspar and is not prone to anomalous fading (Wintle, 1973), an athermal signal loss over time, resulting in age underestimation if not detected and corrected for (e.g. Huntley and Lamothe, 2001). Tests on the single-grain level revealed that only a small amount of quartz grains carries a luminescence signal (~1%). Therefore, the analyses were conducted using multi-grain aliquots with diameters of 2 or 4 mm, respectively, to provide a better yield of equivalent doses and still be close to a single grain level. Because samples from Qurayyah showed feldspar contamination, which could not be eliminated by HF etching, a pIRSAR (post-Infrared single aliquot regenerative or double-SAR) protocol was used (Banerjee et al., 2001; Roberts, 2007) in favour of a standard SAR (single aliquot regenerative) protocol (Murray and Wintle, 2000, 2003; Wintle and Murray, 2006). In a pIRSAR protocol, the first stimulation with infrared light causes the feldspar to emit its charge. A stimulation with blue light follows, targeting the quartz and resulting in the required quartz signal emission, undisturbed by the feldspar. The details of the applied pIRSAR protocol are provided in Table 2a.

All luminescence analyses were conducted on two RISØ TL/OSL DA-20 luminescence reader systems (Bøtter-Jensen et al., 2000, 2003, 2010). For the quartz measurements, blue LEDs (light-emitting diodes, 470 nm) were used to stimulate the luminescence signal, and IR LEDs (875 nm) were used to deplete the feldspar signal. A Hoya U340 7.5 mm optical filter detected the OSL signals in the ultraviolet spectrum (UV). The readers are equipped with a $^{90}Y/^{90}Sr$ beta source submitting a laboratory irradiation dose of ~0.1 Gy s^{-1}. The measurement data were further processed with the software ANALYST (Duller, 2015) and statistically evaluated with the software R and the Luminescence Add-On package (Kreutzer et al., 2012). Radioisotope concentrations (^{40}K and decay chains of ^{238}U and ^{232}Th) were measured using high resolution, low-level gamma spectrometry at the VLL. A Baltic Scientific Instruments (BSI) spectrometer with a high purity Germanium (HPGe) p-type coaxial broad energy detector (~52% efficiency), fitted with a carbon-epoxy window, an ultra-low-background U-type cryostat and a 120 mm low-level lead shielding were used. Dose rate and age calculations were done using the software ADELE (Kulig, 2005). Details on the principles of dose rate and age calculation in ADELE are available from Lüthgens et al. (2017).

Results from radionuclide analyses

Table 1 provides the results from gamma spectrometry measurements conducted after the samples were sealed and stored for at least a month to establish secondary radon equilibrium. All samples were found to be in secondary secular equilibrium.

Results from D_e determination and age calculation

Only those equivalent doses fitting the quality criteria for the applied pIRSAR protocol were used for age calculations. The threshold values were derived from dose recovery experiments conducted to test the chosen pIRSAR protocols' suitability. An application of the following rejection criteria resulted in recovery ratios in agreement with unity within error and a maximum yield of equivalent dose values: recycling ratio/maximum test dose error / maximum recuperation (as a percentage of the natural signal) 10/10/10% for 4 mm and 20/20/20% for 2 mm aliquots. Signals were integrated over the first second of stimulation, and the last 10 s were subtracted as background signal. A typical dose-response and decay curve is shown in Figure 3. Dependent on evaluating the D_e distribution characteristics (KDE-plots of typical dose distributions see Figure 3), the statistical model for the equivalent dose determination was chosen. For all narrow and normally distributed D_e distributions, the central age model (CAM) was used (Galbraith et al., 1999). For those samples showing right-skewed KDE plots and higher scatter of the data (expressed as overdispersion, Table 2), the three-parameter minimum age model (MAM; Galbraith et al., 1999) was applied, because such characteristics indicate incomplete bleaching of the luminescence signal prior to burial. Incomplete bleaching is a common issue occurring in OSL dating of water-lain sediments (e.g. Bailey and Arnold, 2006; Lüthgens et al., 2011; Wallinga, 2002). If incomplete bleaching is undetected and therefore not corrected for, it leads to an overestimation of the calculated age. With the help of the MAM, it was possible to correct the effect of incomplete bleaching effectively when applying a threshold value of σ_b of 0.1 for 4 mm and 0.2 for 2 mm aliquots as derived from the overdispersion values of the well-bleached samples. The results of dose rate and age calculation are summarised in Table 2a.

Table 2. Detailed information on luminescence and radiocarbon ages.

(a) Summary of OSL data and ages.

Area (cf. Figure 1)	Sample (lab code)	Sample (field code)	Grain size (μm)	Aliquot diameter (mm)[1]	Accepted aliquots (n)	Over-dispersion (%)[2]	Qz pIROSL[3] CAM[4] D_e (Gy)	Qz pIROSL[3] MAM[4] D_e (Gy)	Overall Qz dose rate (Gy/ka)[5]	Qz pIROSL CAM age (ka)[5]	Qz pIROSL MAM age (ka)[5]	Age BCE (ka)[6]
E (stone dam)	VLL-0267-L	QU.E.351.S.1	200–250	2	19	18	8.5 ± 0.5	n/a	1.6 ± 0.1	5.5 ± 0.6	n/a	3.5 ± 0.6
	VLL-0268-L	QU.E.351.S.2	200–250	2	17	23	6.3 ± 0.5	n/a	1.3 ± 0.1	4.9 ± 0.6	n/a	2.9 ± 0.6
	VLL-0269-L	QU.E.353.S.1	200–250	2	65	29	n/a	15.9 ± 1.6	2.8 ± 0.2	n/a	5.6 ± 0.7	3.6 ± 0.7
	VLL-0270-L	QU.E.354.S.1	200–250	2	19	31	6.2 ± 0.5	n/a	1.3 ± 0.1	4.7 ± 0.6	n/a	2.7 ± 0.6
	VLL-0271-L	QU.E.355.S.1	200–250	2	31	10	5.0 ± 0.2	n/a	1.3 ± 0.1	3.8 ± 0.4	n/a	1.8 ± 0.4
	VLL-0316-L	QU.E.1001.S.15.L	200–250	2	95	23	n/a	22.0 ± 1.6	3.3 ± 0.3	n/a	6.5 ± 0.7	4.5 ± 0.7
	VLL-0317-L	QU.E.1002.S.15.L	200–250	2	42	35	n/a	16.7 ± 2.0	3.2 ± 0.3	n/a	5.2 ± 0.7	3.2 ± 0.7
J (main inlet)	VLL-0279-L	QU.J.398.S.1	150–300	4	24	10	25.5 ± 0.6	n/a	4.1 ± 0.3	6.3 ± 0.5	n/a	4.3 ± 0.5
	VLL-0280-L	QU.J.399.S.1	200–300	4	23	12	19.9 ± 0.6	n/a	3.6 ± 0.3	5.5 ± 0.5	n/a	3.5 ± 0.5
	VLL-0281-L	QU.J.400.S.1	200–300	4	41	24	n/a	16.6 ± 1.2	3.1 ± 0.3	n/a	5.4 ± 0.6	3.4 ± 0.6
	VLL-0319-L	QU.J.1004.S.1	200–250	4	20	34	n/a	24.5 ± 2.6	1.7 ± 0.1	n/a	14.6 ± 2.0	12.6 ± 2.0
G (canal)	VLL-0275-L	QU.G.371.S.1	200–250	2	16	33	22.4 ± 2.1	17.7 ± 2.2	3.8 ± 0.3	n/a	4.6 ± 0.7	2.6 ± 0.7
	VLL-0276-L	QU.G.372.S.1	200–250	2	8	0	16.3 ± 0.8	n/a	3.4 ± 0.3	4.8 ± 0.5	n/a	2.8 ± 0.5
	VLL-0277-L	QU.G.372.S.2	200–250	2	10	29	15.7 ± 1.6	n/a	3.3 ± 0.3	4.8 ± 0.6	n/a	2.8 ± 0.6
	VLL-0278-L	QU.G.375.S.1	200–250	2	9	16	17.9 ± 1.3	n/a	3.8 ± 0.3	4.7 ± 0.5	n/a	2.7 ± 0.5
F (outlet)	VLL-0272-L	QU.F.362.S.1	200–300	4	20	22	n/a	38.8 ± 4.4	2.1 ± 0.2	n/a	<18.8 ± 2.6	<16.8 ± 2.6
	VLL-0273-L	QU.F.363.S.1	n/a	n/a	n/a	n/a	n/a	n/a	n/a	n/a	n/a	n/a
	VLL-0274-L	QU.F.365.S.1	150–300	4	48	19	n/a	31.0 ± 1.8	4.4 ± 0.6	n/a	<7.0 ±0.7	<5.0 ±0.7
	VLL-0318-L	QU.F.1003.S.1	150–300	4	12	35	n/a	39.6 ± 5.5	4.4 ± 0.4	n/a	<9.1 ± 1.5	<7.1 ± 1.5
	VLL-0370-L	QU.F.1040.S1	150–300	2	19	10	18.3 ± 0.5	n/a	4.0 ± 0.3	4.6 ± 0.4	n/a	2.6 ± 0.4
	VLL-0371-L	QU.F.1041.S2	150–300	2	22	23	n/a	18.2 ± 2.0	3.8 ± 0.3	n/a	4.8 ± 0.7	2.8 ± 0.7

[1] 4 mm aliquots contain approximately 200 grains; 2 mm aliquots contain approximately 50 grains.
[2] Calculated using the central age model (CAM) of Galbraith et al. (1999), using the R luminescence package of Kreutzer et al. (2012).
[3] Measured using a pIROSL SAR protocol using a preheat of 10s@240°C and a cutheat of 10s@220°C, six regenerative cycles applying laboratory doses of ~8 Gy, ~16 Gy, ~31 Gy, ~62 Gy, 0 Gy (recuperation) and ~8 Gy repeated (recycling). The signal was integrated over the first second of stimulation with the last 10s subtracted as background.
[4] Calculated using the CAM and the minimum age model (MAM) of Galbraith et al. (1999) respectively, using the R luminescence package of Kreutzer et al. (2012).
[5] An average water content of 10% ± 5% was included in the doserate calculations as a representative average water content since burial. Dose rate and age calculations were conducted using the software ADELE (Kulig, 2005). Details concerning dose rate calculation with ADELE can also be found in Lüthgens et al. (2017).
[6] The respective MAM and CAM luminescence ages refer to the date of measurement as a reference and were converted to ages BCE to make comparison in the archaeological context more straightforward.

(b) Summary of radiocarbon data and ages.

Area (cf. Figure 1)	Sample (lab code)[1]	Sample (field code)	Type of dated material	[14]C age (years BP)	Calibrated age BCE (a)[2]
M (mesa)	UGAMS 35,790	QU.M.864.S.1	Charcoal (tamarix)	4070 ± 25	2849–2492
	UGAMS 35,791	QU.M.870.S.4	Charcoal (tamarix)	4060 ± 20	2835–2492
	UGAMS 35,792	QU.M.873.S.2	Wood (tamarix)	4050 ± 25	2833–2487
J (main inlet) yardang	UGAMS 52,099	QU.J.1005.S.1	Melanoides cf tuberculata	10,890 ± 30	10,929–10798
	Poz-136429	Q15-4 : 0–5 cm	Bulk organic carbon (0.05 mg) from silty gypsum	9510 ± 160	9284–8429
	Poz-136430	Q15-4 :40-45 cm	Bulk organic carbon (0.5 mg) from silty gypsum	6220 ± 35	5303–5051
	Poz-136431	Q15-4 : 125–130 cm	Bulk organic carbon (0.1 mg) from silty calcite	21,000 ± 250	23,899–22,733
	Poz-136432	Q15-4 : 175–180 cm	Bulk organic carbon (0.09 mg) from fine sand	19,100 ± 210	21,786–20,567

[1] Sample preparation and AMS (accelerator mass spectrometry) conducted at University of Georgia (UGAMS) (Cherkinsky et al., 2010) and the Poznan Radiocarbon Laboratory (POZ) (Goslar et al., 2004).
[2] Calibrated using OxCal v4.2.4 (Ramsey and Lee, 2013); IntCal 20 Reimer et al., 2020); age ranges represent 2σ uncertainties.
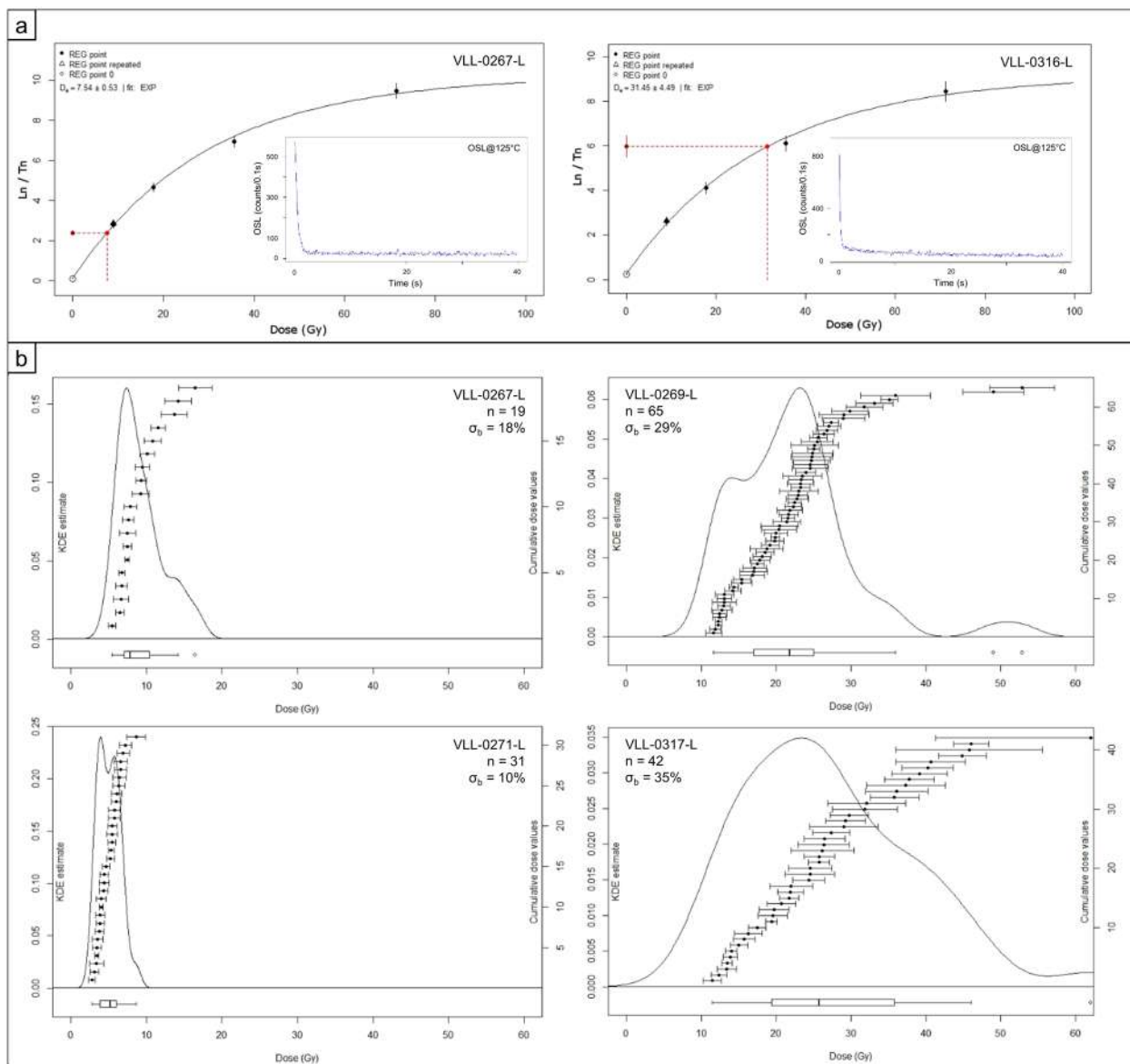
Figure 3. Typical luminescence properties of the investigated samples: (a) Dose response curves (sensitivity corrected luminescence signal Ln/Tn plotted over dose) for samples VLL-0267-L (left) and VLL-0316-L (right) showing exponential growth of the luminescence signals. The insets show shine-down curves of the OSL signal stimulated at 125°C, with the rapid decay showing that the signal is dominated by the fast component of quartz and that the signal contribution from feldspar was successfully depleted beforehand as intended using the pIROSL protocol. (b) Typical dose distributions for four samples showing the cumulative dose values, kernel density estimates (KDE) and box plots illustrating the differences in scatter between well bleached samples on the left (top: VLL-0267-L, bottom: VLL-0271-L) and poorly bleached samples on the right (top: VLL-0269-L, bottom: VLL-0317-L).

Reliability and significance of luminescence ages

The ages provided in Table 2a were analysed with regard to their reliability and significance for the date of the erection of the respective buildings to provide reliable ages for the construction of the key sites.

- Area G (canal): All four samples taken at this site show excellent agreement of the ages within error. Sample VLL-0275-L was identified as incompletely bleached. However, the age based on the MAM calculation successfully corrects any overestimation by incomplete bleaching, resulting in an age in agreement with the three well-bleached samples. The four samples average age (mean ± standard deviation) is 4.7 ± 0.1 ka (2800–2600 BCE). Because the sampling spots nicely bracket the construction, this average age represents a construction age for the water canal.

- Area E (stone dam): Five samples at this site were taken directly at the dam structure (VLL-0267-L to VLL-0271). The ages of these samples agree within error and follow a general trend from old to young in stratigraphic order, providing strong evidence for high reliability of the dates. The age of sample VLL-0269-L represents the only deviation from this trend, but it is still in agreement with the over- and underlying ages within error. However, as that sample was identified as incompletely bleached, the two well-bleached samples (VLL-0268-L and VLL-0270-L) best constrain the construction age. Therefore, we calculated an average age of 4.8 ± 0.1 ka (2900–2700 BCE) for the construction of the dam structure, which is in excellent agreement with the age calculated for the site above (Area G). Samples VLL-0316-L (6.5 ± 0.7 ka; 5200–3800 BCE) and VLL-0317-L (5.2 ± 0.7 ka; 3900-2500 BCE) were sampled in close vicinity of the dam from the topmost decimetres

of sediments representing Wadi Ghubai's bed and the wadi sidearm's bed. The resulting ages are in good agreement with the samples taken in similar depths directly below the dam structure (VLL-267 & VLL-268). These results imply that the dam was constructed atop the natural wadi surface and no significant sediment aggradation happened since then at the site.

- Area J (main inlet): Four samples were taken at this site, with two samples showing signs of incomplete bleaching, which we accounted for in age calculation by the application of the MAM. The resulting ages show good agreement within error for the top three samples (VLL-0279-L to VLL-0281-L) and a significantly higher age for the sample taken at the inlet's base (VLL-0319-L). The topmost sample VLL-0281-L yields an age of 5.4 ± 0.6 ka (4000–2800 BCE) and was taken from a stratigraphic unit (SU 400, Figure 2) which may be interpreted as consisting of mudbricks even if they were difficult to identify with certainty. While colour and texture align with those expected for mudbricks – as amply documented elsewhere in Qurayyah (Luciani, 2016, 2019, 2021a, 2021b) – no discontinuities interpretable as mortar could be detected. This could be due either to incipient paedogenesis blurring original structures or the use of adobe rather than parallelepiped-shaped bricks. If the latter were confirmed through excavation, it would mean that we have a localised anthropic construction in this position. Moreover, the average age of all three upper samples of 5.8 ± 0.4 ka (4200–3400 BCE) is in good agreement with the ages calculated for the previous site's wadi deposits (Area E). The age of 14.6 ± 2 ka (14600–10600 BCE) at the inlet's base represents a natural deposit from the Late Pleistocene. This indication is corroborated by the occurrence of multiple snail shells in this layer. For one of these (QU.J.1005.S.1), we obtained a radiocarbon age (compare Table 2b) discussed in the subsequent chapter. While the upper ages (VLL-0281-L and VLL-0280-L) partially overlap the ones established for the sites above (Area E and G), like the lowermost samples from Area F (below), the Area J samples document a significantly older part of the geomorphological stratigraphic sequence than Areas E and G.

- Area F (outlet): As in inlet Area J (above), the samples had to be taken from material that must be regarded as part of the structure itself. The three samples from the base of the structure which yielded sufficient material for luminescence dating purposes (VLL-0272-L, VLL-0274-L, VLL-0318-L) all show clear indications of incomplete bleaching, and the resulting ages are randomly scattered, although the MAM was applied. In contrast to the previous sites, these ages must be regarded as unreliable from a methodological perspective and do not provide information about the structure's building period. This information leads to two hypotheses. Either the base of the structure is entirely human-made, and the material was not sufficiently bleached during the construction process, or, more likely, the building's core is a form of natural sediment included in the outer wall, such as, for example, a relict yardang (Dinies and Hoelzmann, 2020) and inlet Area J (above). Sample VLL-0274-L at least provides the information that the structure must be younger than 7.0 ± 0.7 ka (5700–4300 BCE). Two additional samples (VLL-0370-L, VLL-0371-L) were taken from sandy material sandwiched between anthropogenic layers of unhewn stones in the top part of the structure (Figure 2). In contrast to the samples taken at the base of the structure, the latter show much better bleaching characteristics with only VLL-0371-L showing minor indications of incomplete bleaching, which could be corrected by applying the MAM. Both samples yield ages in agreement within error, resulting in an average age (mean $\pm$ standard deviation) of 4.7 ± 0.1 ka (2800–2600 BCE). Because the samples were taken directly from the material forming the upper part of the structure, we interpret this age as a construction age. The agreement of the ages of both samples and the good bleaching characteristics indicate that the material was sufficiently bleached during the construction process. Otherwise, we would have expected the data from these samples to show the same scatter as observed from the samples taken at the base of the outlet structure. The construction age of the upper part of the outlet structure is in excellent agreement with the ages determined for the construction of the canal (area G) and the stone dam (area E).

The OSL ages provide reliable evidence that the structures at the key sites in Areas E (stone dam), G (canal) and F (outlet) were constructed in the Early Bronze Age, most likely at around 2900–2600 BCE. The ages determined for the sequence in area J (main inlet), as well as the minimum ages determined at the base of the outlet structure of area F support the above reconstruction and also provide evidence on more ancient deposits of the local geomorphological sequence, which agree with off-site yardang dates (see below). Additional samples providing a chronology for structural elements within the walled area were already secured and remain to be analysed in future studies.

Age crosscheck using radiocarbon dating

In addition to the OSL ages, radiocarbon dating was applied at a key site on the Rock Plateau (mesa). A semi-circular, engaged stone tower was investigated through systematic, controlled stratigraphic excavations (Area M, Figure 1b; Luciani, 2021b). Since the stone tower leans onto the western façade of the eastern cross-wall, dating its use allows obtaining a date for the construction of the tower, the cross walls on the Rock Plateau and – if we accept their likeness with the general town walls encircling the agricultural area – the foundation of the entire settlement.

Radiometric measurements were conducted on charcoal and wood samples of tamarix, stemming from Phase 8 deposits (samples UGAMS 35790-35792), the most ancient excavated inside the tower (Area M, Luciani 2021b). The results from radiocarbon dating (Table 2b) are in perfect agreement with the ages derived from OSL dating and provide excellent proof of the construction of key sites of the settlement to the Early Bronze Age II-III. Radiocarbon ages from two overlying layers inside the tower as well as two human remains in an adjoining stone burial in the mid-third millennium calBCE constrain and confirm these early dates.

Additional radiocarbon ages further corroborate the results from OSL dating and allow for a deeper insight into the landscape history of the Qurayyah area. A sample (UGAMS 52,099) from one specimen of *Melanoides cf tuberculata* (Figure 2c) taken from stratigraphic unit SU396, slightly above the base accumulation in Area J, yielded an age of 10929–10798 calBCE, which is in good agreement within error with the OSL age determined for that stratigraphic unit. This contemporaneity implies that the sediment was deposited shortly after the snail shell incorporated the ^{14}C, and was not disturbed subsequent to burial and is therefore still found to be *in situ*. Although *Melanoides cf tuberculata* is a freshwater snail, the sample was not tested for hard-water effect, which may lead to age overestimation of radiocarbon ages. However, the agreement of the radiocarbon age with the OSL age indicates, that no significant hard-water effect

was present in the sample. Four radiocarbon ages of the organic fraction were determined for samples from a yardang in the area downstream after the drainage from Qurayyah unites with wadi Ghubai, about 4 km to the NNE from the main outlet (Figure 1g). This site was previously shown by Dinies and Hoelzmann (2020) and detailed information of the analyses conducted at this site is provided as supplementary material S2. Despite some age inversion present in the dataset, which is most likely caused by the very low amounts of organic carbon available for dating (Table 2b), these ages confirm the deposition of sediments in a playa-like landscape in the broader Qurayyah area from the Late Pleistocene to at least early-Holocene, but most probably even up to Mid-Holocene times. These results can be nicely correlated with the time frames determined for the basal deposits in Area J and the material from the lower part of the outlet structure in Area F.

Interpretation of the functionality of the investigated key structures

The ages determined for the key infrastructure of the settlement – the dam upstream of the site (Area E), the monumental cross walls on top of the Plateau (Area M), the canal channelling fracture-spring water from the karstic system at the bottom of the Plateau (Area G), the outlet (Area F) and most likely the inlet (Area J) of the agricultural area – coherently fall into the same time frame in the Early Bronze Age. It is at this point that we see the construction of the oasis' monumental walls and water harvesting infrastructure as a result of a coordinated effort to establish a permanent settlement and a related system for managing its surface water resources, in an area covering several hundred hectares.

In order to check the functionality of the entire irrigation setup, we mapped the system's key structures and main waterways through the oasis and its close surroundings. Here, we are building on the Hüneburg et al. (2019) survey. Based on this geomorphological map and the position of the investigated structures within the geomorphological setting and paleo-hydrological system, we assigned each structure to one of three different technical classes with a proposed hydrological function: (1) Diversion, Storage and Retention, (2) Transfer, (3) Capillary distribution. These elements were scrutinised by detailed mapping during a field campaign, including surveying of new structures of the irrigation system located in the irrigation canals bed and their close surroundings not previously documented.

A GEOEYE satellite image was used for the preliminary analysis before the fieldwork to identify features and determine areas of interest for closer investigation on the ground. The locations of all identified structures were documented using handheld GPS (global positioning system), and the dimensions of all structures were surveyed with measuring tape in the field. Additional to field mapping, drone photography was used at selected locations along one of the central irrigation canals through the agricultural area. Our study aims to correlate the investigated sites and the respective human-made constructions' functionality into an integrated conceptual model.

Description and interpretation of the key structures of the SWHS

The following main elements (upstream to downstream) of the SWHS were identified (overview see Figure 1, details see Figure 4):

- The human-made structure in Area E (Figure 1b, Figure 4b) represents the most upstream water-harvesting-system element and is interpreted as a diversion dam (technical class 1). It is a linear structure situated along the right bank of Wadi Ghubai (oriented from SSE to NNW) with an approximate length of 300 m. The dam's position diverted the Wadi Ghubai from its sidearm, deflecting the main water masses away from Qurayyah. At least two openings ensured that parts of the runoff still reached Qurayyah. When Wadi Ghubai's water table rose above the dam's height, it is possible, that it additionally functioned as an overflow weir. The dam is positioned on a terrain edge, caused by Wadi Ghubai's height difference to the sidearm's bed. The sidearm's bed is situated at a higher altitude than Wadi Ghubai's bed. This edge has an approximate height of 70 cm along the entire length of the diversion dam. Today, only the dam's base is still intact (Figure 4b). Blocks made of sandstone, most likely originating from the neighbouring environment, were used for the erection of the dam. Because of its poor state of preservation, it is impossible to reconstruct the dam's original height reliably or the original position and shape of possible openings in the dam.

- Downstream from the dam in Area E (i.e. further to the north), water flow was directed towards Qurayyah through the side valley branching from the Wadi Ghubai. In this side valley, a prominent line of sandstone blocks oriented in SSW to NNE direction crosses the wadi bed (Figure 4a, Figure 4c). Up to now, it remains unclear whether these blocks fulfilled a hydro-archaeological function.

- An opening (Area J) through the west-east wall bordering the oasis in the south, is a human-made structure and interpreted as main inlet (Figure 4a, Figure 4e) (technical class 1). Today, it is a 14 m broad opening through the approximate 4 m high outer mudbrick wall. A single line of stones, also oriented west-east with an approximate length of 4 m is recognisable at the centre of the opening's base/floor. This stone partition is interpreted as a retaining stone hurdle, limiting the inlet's cross-section, hence regulating its flow rate. Lessening flow velocity was essential for retaining the water in front of the main inlet, reducing the effect of erosion, and protecting the irrigation canals inside the walled area (technical classes 2 and 3) from damage. The retention delayed the progress of the water through the oasis, extending the time of its availability and infiltration.

- A similar opening, in the stone and mudbrick wall oriented southwest-northeast, can be found close to the Residential Area (Figure 4a, Figure 4f, next to excavation Area R). We propose that this structure represents a subordinate side inlet for conveying surface water into the settlement area (technical class 1). Today's width is 11 m. Like the main inlet, this opening also features a single stone line at the centre of the opening's floor. This line has a length of approximate 2.5 m, is oriented southwest-northeast and may also be interpreted as retaining stone hurdle as the one at the main inlet. The reduction of the velocity of the water flow had great importance at this inlet because of its vicinity to the funerary complex (Luciani, 2021a) bordering the wadi shore (Area R).

- The human-made structure in Area G (Figure 4a) is interpreted as a water canal (Figure 4d). It extends from a basin, very likely collecting water from the fracture springs (initially mentioned but not identified by Ingraham et al., 1981, and recently rediscovered and described by Hüneburg et al., 2019) to the inner part of the settlement, oriented southwest-northeast (technical class 2). The canal features vertical stone slabs as canal walls and no flooring. The canal had an average width of around 75 cm, a maximum height
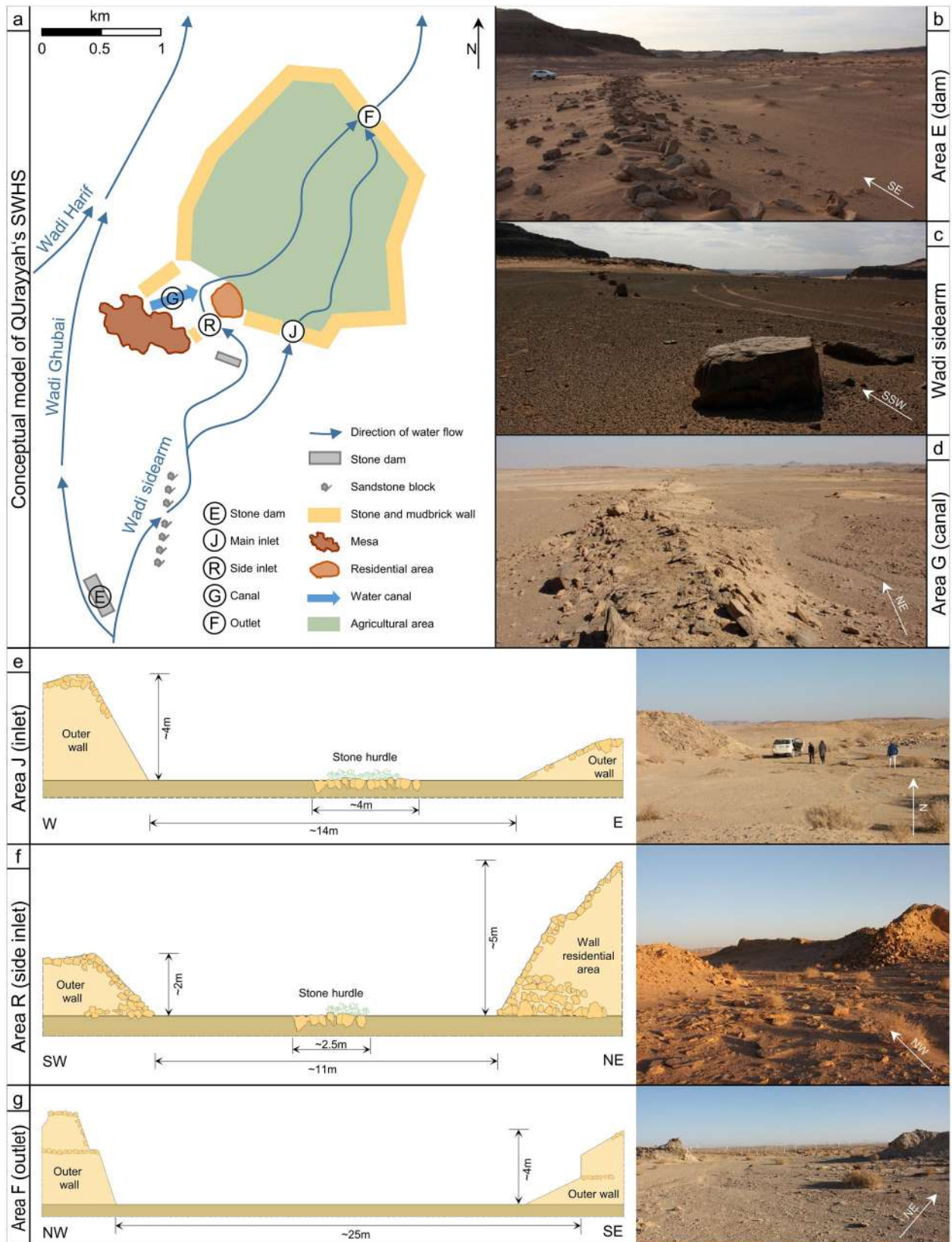
Figure 4. (a) Simplified flowchart depiction of the key elements of the proposed conceptual model of the SWHS of Qurayyah. (b) Photo showing the remains of the main stone dam (Area E) located on a small terrace step separating Wadi Ghubai from the wadi sidearm leading to Qurayyah. (c) At about half the distance between the main stone dam and the settlement wall of Qurayyah, as shown in the photo, sandstone blocks are arranged in a linear fashion, crossing the wadi sidearm from SSW to NNE. (d) Photo of the remains of the water canal, leading from the fracture spring on the northern side of the mesa towards the residential area. (e) Technical sketch and photo of the main inlet (Area J). (f) Technical sketch and photo of the subordinate inlet close to Area R, showing the higher mudbrick wall of the adjacent Residential Area on the right. (g) Technical sketch and photo of the outlet (Area F). All technical sketches include measured dimensions based on today's degree of preservation of the structures. Therefore, they may not represent the original dimensions, but the best available approximation for subsequent runoff calculations. All photos taken by C. Lüthgens in 2017.

of 65 cm and a length of at least ca. 300 m as reconstructed from its remains visible on today's surface.

- At Area F, the human-made structure related to the SWH-system was interpreted as main outlet (Figure 4a, Figure 4g) for the residual water exiting the walled area (technical class 1), oriented northwest-southeast. The outlet represents the most downstream key feature of the system. Today, it has a width of 25 m. The walls flanking the outlet have an approximate height of 4 m. A stone hurdle, as detected at the centre of the inlets, is missing. Here the basal sandstone (bedrock) is exposed at the surface. Any potential structure must be considered as lost to erosion.

A conceptual model for the SWHS at Qurayyah

Summarising the interpretations of the key elements, we propose that the described structures are part of a complex SWHS described by the conceptual model summarised in the flowchart in Figure 4a.

The dam, Area E, marked the entry point of the SWHS towards the oasis (Figure 4b). It was strategically positioned about 2 km upstream of the settlement walls at a site where a sidearm originated from Wadi Ghubai, flowing towards the oasis (Figures 1b and 4a). As described above, the dam is positioned on a terrain edge. Due to this edge, Wadi Ghubai had to carry a minimum water quantity with a water table height of approximately 70 cm to overcome this obstacle and activate the water supply to the SWHS.

About half the distance between the main dam in Area E and the outer wall of the settlement, the bed of the wadi sidearm splits into two streams, with the eastern one directed towards a main inlet (Area J) and the western one towards a side inlet close to Area R. It remains unclear if and how the alignment of short pilasters (Figure 4c) may have influenced the flow of surface water in the wadi sidearm. An additional subordinate stone dam located about 300 m to the SE of the inlet close to Area R is oriented at a right angle to the stream direction in the wadi and potentially functioned as a further diversion dam to reduce the stream power and protect the side inlet close to the residential area (Figure 4f). The runoff, which entered the walled oasis area through the main inlet, Area J (Figure 4e), provided water for irrigation purposes. The other fraction of water which entered through the smaller side inlet near the Residential Area, Area R (Figure 4f), possibly mainly contributed water for drinking, residential and productive activities. The function of both inlets was to regulate the amount of water entering the settlement. Inlets also protected the agricultural and residential areas from potential damage caused by flooding events.

In addition, this first retention had the effect that it took the water longer to cross the oasis area before reaching the outlet, allowing the residents to use it for a longer time. From the main inlet (Area J), irrigation canals channelled the water into the agricultural area. The stream originating at the side inlet (close to excavation Area R) flowed past the Residential Area and pottery production zone before irrigation canals also guided it to the agricultural area. Here, a plethora of remains of structures, such as subordinate irrigation canals and walls, were identified. Due to prevailing erosive processes, many constructions are still clearly visible in the field. Already Parr et al. (1970) (but even more Ingraham et al., 1981) differentiated them into low walls and irrigation canals due to their shape. However, a detailed analysis of the irrigation structures (technical class 3) is beyond this study's scope. They will be investigated more closely in the future.

The outlet (Area F) was located downstream, in the north of the settlement (Figure 4g). Being the only way for the water to exit the oasis, the outlet constituted a bottleneck for the outflowing water.

The water canal in Area G (Figure 4d), was most likely used to supply the settlement with drinking water from the fracture springs, located north of the plateau. The quality of that karstic spring water was likely very high compared to surface runoff water. Therefore, the usage as drinking water seems highly plausible. However, the quantities of water from these springs can be assumed to have been relatively low. Most likely, the springs did not contribute a significant amount of water for irrigation purposes or pottery production. However, it remains to be clarified if and how the canal in Area G was connected to the overall SWHS.

In summary, Qurayyah's SWHS uniquely combines elements of different wadi farming techniques described by Reilly (2015), with most similarities to be found with systems described as large scale wadi farming (dam structures routing the water to major canal structures), *sayl* diversions farming (diversion of water for controlled flooding of farming areas) and *sayl* farming in a wadi delta (artificial inlet structures controlling the routing of water to the agricultural areas), respectively.
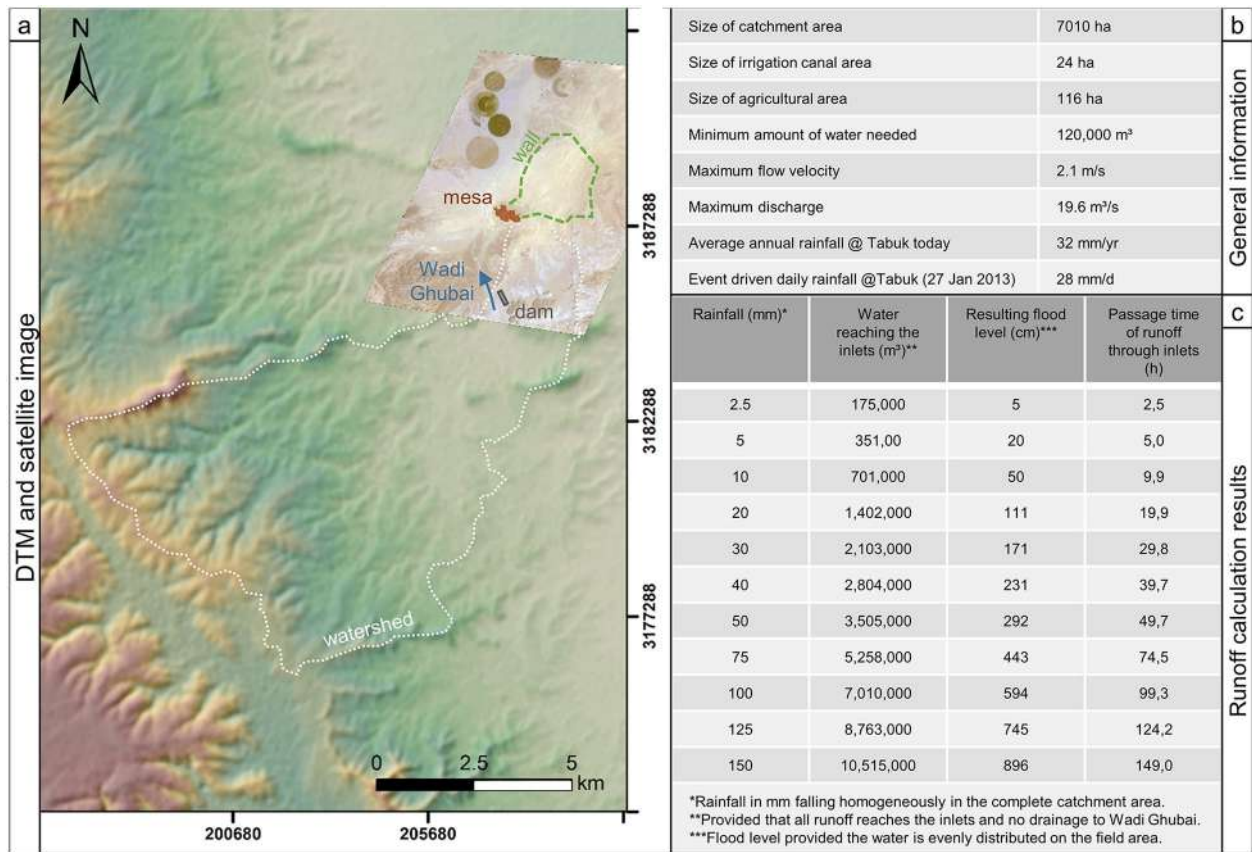
Plausibility check of the SWHS

We provided a conceptual model for the SWHS's functionality based on a reliable chronology for its construction. In this final step, we aim to test the plausibility of the proposed conceptual model's functionality. The goal is to clarify if the catchment area of Wadi Ghubai could generate a runoff volume big enough to supply the SWHS with enough water to irrigate the fields. Therefore, we calculated the water quantity reaching Qurayyah during rainfall scenarios with different amounts of precipitation.

Experimental setup

All calculations were based on basic parameters derived from a pan-sharpened GEOEYE satellite image, and an ASTER Global DEM Version 2 (GDEM2 in GeoTIFF format with Universal Transverse Mercator Zone (UTM R37) projection and WGS (World Geodetic System) 1984 horizontal datum). ArcMap 10.6 was used for pan-sharpening the satellite image to generate a multiband-grid layer with the panchromatic layer's high resolution. From these basic data, the irrigation canals and the agricultural area inside the settlement walls were mapped, and the surface areas were calculated. Additionally, the catchment area of Wadi Ghubai was calculated from the ASTER dataset using Arc Hydro Tools. In a first step, all depressions were filled to generate a coherent stream system for the entire catchment area. Subsequently, a grid was generated, which identified each cell's flow direction based on the underlying digital elevation model. A stream network was generated in using the Standard-Strahler-Method. For the calculation of the size of the catchment area, the inlet (Area J) was defined as the pouring point and all runoff from the catchment was routed to the settlement area using the watershed layout shown in Figure 5, pretending that runoff through Wadi Ghubai was not possible. ArcMap calculates the catchment area for a set geographical point with the determined flow direction and stream order.

Based on the size of the catchment area, the potential runoff reaching the pouring point (the inlet, Figure 5) was calculated for different precipitation scenarios, assuming uniform precipitation in the catchment area. Effects of evaporation, infiltration and the dam's diversion function are not included in this simplified first verification of the SWHS.

The last step was to verify for which precipitation scenarios the amount of water provided from the catchment area of Wadi Ghubai

Size of catchment area	7010 ha
Size of irrigation canal area	24 ha
Size of agricultural area	116 ha
Minimum amount of water needed	120,000 m³
Maximum flow velocity	2.1 m/s
Maximum discharge	19.6 m³/s
Average annual rainfall @ Tabuk today	32 mm/yr
Event driven daily rainfall @Tabuk (27 Jan 2013)	28 mm/d

Rainfall (mm)*	Water reaching the inlets (m³)**	Resulting flood level (cm)***	Passage time of runoff through inlets (h)
2.5	175,000	5	2,5
5	351,00	20	5,0
10	701,000	50	9,9
20	1,402,000	111	19,9
30	2,103,000	171	29,8
40	2,804,000	231	39,7
50	3,505,000	292	49,7
75	5,258,000	443	74,5
100	7,010,000	594	99,3
125	8,763,000	745	124,2
150	10,515,000	896	149,0

*Rainfall in mm falling homogeneously in the complete catchment area.
**Provided that all runoff reaches the inlets and no drainage to Wadi Ghubai.
***Flood level provided the water is evenly distributed on the field area.

Figure 5. Summary of the plausibility check of the SWHS at Qurayyah. (a) Digital terrain model (DTM) based on ASTER Global DEM Version 2 (GDEM2), Universal Transverse Mercator Zone (UTM R37) projection and WGS (World Geodetic System) 1984 horizontal datum; colour palette indicates elevation ranging from ~1300 m asl (brown) to ~700 m asl (light green). The inset shows a pan-sharpened satellite image acquired on 15 September 2015, GEOEYE sensor Digital Globe (licenced to the University of Vienna). The dotted white line indicates the watershed used for the runoff calculations. Outflow to wadi Ghubai (blue arrow) was blocked for the calculations. For better orientation, some major elements of the SWHS and the settlement are depicted: stone dam (grey), mesa (brown), encircling wall (dashed green line). For details, please see Figures 1 and 4. (b) General information on basic parameters used for calculation, maximum velocities and discharge values calculated, and average annual rainfall and recorded event driven daily rainfall for Tabuk under today's climatic conditions (from Abushandi, 2016). (c) Results from runoff calculations for different rainfall scenarios.

is sufficient to flood the agricultural area. The basic working hypothesis is that the irrigation canals must be filled with water to overflow their banks and flood the adjacent fields. This water volume inside the irrigation canals is critical for flood irrigation and is seen as a minimum water quantity needed. All water delivered in addition to this minimum will flood the agricultural area.

The required minimum water volume was calculated by multiplying the previously determined irrigation canal areas (24 ha) with a water height of 0.5 m. This height was determined through previous research (Parr et al., 1970, assumed a max. height of 70 cm for walls built in this period on the fields) and own field observations, which confirmed 50 cm as a valid threshold. This minimum water volume was subtracted from the overall amount of water reaching the Main Inlet (Area J). The remaining amount of water was divided by the size of the agricultural area (116 ha), providing a flood height for each precipitation event.

In addition, the Gauckler-Manning-Strickler equation was used to calculate the maximum flow velocity through the inlets. This equation is a simplified formula that is well-suited to calculate the maximum discharge and flow velocity through simply shaped profiles, (Bollrich, 2013). Current dimensions of the main inlet (Area J), the side inlet (Area R) were taken as reference for these calculations (Figure 4e/f), as the closest approximation to the original structures. With the determined flow velocity, it is possible to estimate the time needed to fill the irrigation system with water and flood the agricultural areas.

Results of the plausibility check

The results of the plausibility check are summarised in Figure 5b and c. It also shows the minimum amount of water required to reach the inlets in order to enable irrigation of the agricultural areas, as well as the maximum flow velocity and maximum discharge through the inlets. The precipitation height per event, the resulting amount of water reaching the main inlet, and the flood height (rainfall equivalent) depended on the amount of precipitation, as well as the time needed for the water to pass the inlets (Figure 5c).

The calculation results show that a small amount of precipitation generates a high amount of potential runoff from the catchment area to Qurayyah. For example, a rainfall event of 5 mm would generate a flood height of 20 cm on the agricultural area, which can be translated to a precipitation equivalent of 200 mm over the agricultural area. Here must be stressed that the plausibility check is based on maximum scenarios by not allowing any runoff to bypass Quaryyah via wadi Ghubai. In addition, the plausibility check does not include loss of water volume by infiltration or evaporation. However, these maximum runoff scenarios clearly demonstrate that the catchment area is not only able to generate sufficient amounts of runoff to sustain the SWHS even during minor rainfall events, but that it may even generate massive flood events had all water been routed towards the settlement area. The results corroborate the hypothesis that the stone dam (Area E) was built as a diversion dam to control the amount of water that could

enter the wadi sidearm from Wadi Ghubai, hereby preventing catastrophic flooding of the oasis. Even under today's arid climatic conditions, rainfall events reaching almost 40 mm of precipitation per day (in contrast to an average annual rainfall of only 32 mm at Tabuk today) have been observed in the Tabuk area (Abushandi, 2016). A comparable event would generate an amount of more than 2.8 million m³ of potential runoff in the catchment area used for the plausibility check (Figure 5) and would have resulted in a catastrophic flooding level of almost 3 m had it reached the agricultural area in full quantity. In summary, the plausibility check successfully verified the functionality of the SWHS of Qurayyah as proposed in the conceptual model and highlights the key function of the stone dam for flood prevention.

Contextualising Qurayyah's SWHS

The nearest climate archives (shown on Figure 1a) to Qurayyah provide information about the last climate optimum in the broader region. On a millennial scale (sinusoidal cycles of ~1.5 ka), the speleothem record of Soreq Cave (Bar-Matthews and Ayalon, 2011) indicates a dry period at the beginning of the Early Bronze age, roughly coinciding with a change to more arid conditions in the area as reconstructed by Whitney et al. (1983). The youngest dry event documented in Soreq Cave also coincides with a major evaporation event documented in a marine core from the Northern Red Sea at around 4200 cal yr BP (Arz et al., 2006). At Rasif (Zielhofer et al., 2018) increasing salinity in *qa* sediments starting during the fifth millennium BCE may be interpreted as an onset of aridification at the site. Latest results from the analysis of sabkha deposits from Tayma indicate a considerably shorter wet period in Northern Arabia, only lasting from 8800–7900 yr BP as opposed to the more commonly defined Holocene Humid Period lasting up to about ~5500 years BP (Neugebauer et al., 2022). Within this palaeoclimatic framework, our dating results show that the SWHS of Qurayyah was established during a period of climate change on a landscape surface, which was formed up to about ~6.5–5.5 ka (~4500–3500 BCE) (Area E, stone dam and Area J, main inlet), with anthropogenic constructions of the SWHS probably documented as early as 5.4 ± 0.6 ka (4000–2800 BCE) (potential mudbricks in Area J, main inlet). The construction of the major elements of the SWHS fall into a short period as documented by the well-defined construction ages of the stone dam (Area E) at 4.8 ± 0.1 ka (2900–2700 BCE), the canal (Area G) at 4.7 ± 0.1 ka (2800–2600 BCE), and the outlet (Area F) at 4.7 ± 0.1 ka (2800–2600 BCE). In Qurayyah, establishing a SWHS was the topographic precondition for developing the architectural layout of a complex settlement in the low laying playa and the economic basis for watering the fields that fed the large population of the site and integrating local sources (the Plateau's fracture springs, Hüneburg et al., 2019) of drinking water. No urban-sized settlement can develop without sufficient exploitable water and a sustaining agricultural hinterland (Luciani, 2021b; Mazzoni, 1997). Two millennia after their foundation, in the Late Bronze Age, Qurayyah's hydraulic structures were also part of a well-developed symbolic and cultic landscape (Luciani, 2021a).

Table 3 summarises the main investigated sites in Northern Arabia and the Southern Levant with relevant watering systems, listing locations, geomorphological and hydrological properties, and additional information about their water supply systems.

Table 3 shows that most of the locations had a perennial supply of water due to springs (Table 3 no. 7), qanats or wells. Dependent on the hydrological situation, some oases used a combination of these structures. In Tayma and Al-Ula (Table 3 nos. 6 and 10), a blend of groundwater usage and a water harvesting system was used to allow maximum exploitation of the water resources. Tayma and Dumat al-Jandal (Table 3 no. 9), for example, used the ephemeral river system (wadis) to refill their sabkhas. For Tayma, Engel et al. (2012) reconstructed an average annual rainfall of 150 ± 25 mm to sustain this system during the early Holocene.

In contrast to these oases, only Qurayyah, Jawa and the Jafr basin were dependent exclusively on surface water/wadi system's water supply, with no accessible natural reservoirs, such as sabkhas or endorheic basins (locally called *Qa'as*).

The comparison of additional properties underlines Qurayyah's unique situation. Jawa and the Jafr Basin (Table 3 nos. 1–2) irrigated limited agricultural areas by means of small-size water storage systems that were built locally (Fujii et al., 2017; Meister et al., 2017). In the Jafr basin, the barrages collected only enough water to supply a small cistern and a stand-alone field at outposts during the PPNB (Fujii et al., 2017), significantly earlier than Qurayyah or Jawa. In Jawa (3500–3000 BCE), runoff-terraces, dams and pools were used to irrigate 38 ha of fields and to store the water in reservoirs (Meister et al., 2017, 2018a).

According to our dates, pointing to the early third millennium BCE (Table 2) for the construction of this sophisticated system securing and managing water supply for a settlement bounded by monumental architecture, we can say Qurayyah's SWHS is the oldest of its kind and breadth. The only oasis with a similar field extension to Qurayyah is Ein Ghedi (Table 3 no. 5). However, this is the only similarity between these two oases. Several active springs were used to supply the latter with water. The maximum size of 110 ha was reached during the Roman-Byzantine period (Hadas, 2012), which stands in significant contrast to Qurayyah, which had its maximum extent during the Bronze Age.

At Rasif (Zielhofer et al., 2018) around 4.6–3.9. cal BCE most distinctive well and trough structures were constructed within endorheic basins (so-called *Qa'as*). This is about 1000 years earlier than at Qurayyah, with a significantly smaller spatial dimension and a postulated use for pastures, instead of irrigated fields as in the oasis (Table 3).

Qurayyah's (Table 3 no. 4) unique situation is given by the latitude of a water control system extending to several kilometres upstream from the actual agricultural area that needed water supply, thus making it not a local but a micro-regional SWHS and because it was developed for the needs of the urban-sized settlement, characterised by an anthropic landscape defined by monumental architecture.

Such an ample and complex SWHS allowed to provide water within a quasi-planar area in a playa like landscape with no terraces, at a distance of ~2 km from the main surface water source (Wadi Ghubai), sustain a 300 ha large settlement including the remarkable size of 116 ha agricultural fields inside the settlement's walls and several additional hundreds of hectares outside of the city walls.

Table 3. Synoptic table of the main characteristics of investigated water supply systems in the North Arabian Peninsula and the Southern Levante.

	Location	Geomorphology	Water source	Water usage	Irrigated area	Additional info	References
1	Jafr Basin, Jordan SE Jordan PPNB	It is a large depression of 15.000 km², 900 m a.s.l. in altitude at the centre and 1200 m a.s.l. in the surrounding hills and an internal closed drainage system. Qaʿas (seasonal, local depression filled with water and fine deposits) are spread over the flint pavement desert.	Ephemeral river system (wadi)	The grouping of a basin-irrigation barrage, a cistern and an outpost is a so-called 'triple set'. This triple set is related to a flat terrain or playa.'Triple sets' were found in the Jafr Basin at Wadi an-Nuʿaydiyyah, Wadi Ghuwayr, Wadi Nadiya and Wadi Abu Tula.	2–3 ha	The cistern was used to collect drinking water. The basin irrigation barrages irrigated an adjacent field. Different barrage types were used. For example, large scale barrages induce extended shallow flood areas for the basin-irrigation of a single field. It is linear and located at a small- to medium scale drainage system. In contrast, semi-circular barrages for long-term water accumulation are found across a small gully or shallow depression.	Fujii and Abe (2008), Fujii et al. (2011, 2012, 2013), Fujii (2014), Fujii et al. (2017)
2	Jawa, Jordan N 32°20′9″ E 37°0′7″ 1st occupation phase 3500-3000 BCE 2nd occupation phase ~2000 BCE	It is situated in the basalt desert steppe, on Wadi Rajil at 1002 m a.s.l. altitude. Qaʿas are commonly found between the hills of the surrounding undulating plain.	Ephemeral river system (wadi)	An elaborate, terraced runoff, water distribution and storage system was used to harvest the surface water delivered by the Wadi Rajil and the surrounding hillslopes. Pools, dams, canals and five water reservoirs were used.	38 ha	The terraced runoff system utilised the surface and flood water to irrigate the agricultural terraces. Stone walls border the terraces.	Meister et al. (2017, 2018a, 2018b), Müller-Neuhof et al. (2013, 2015)
3	Rasif, Saudi Arabia NE Saudi Arabia	Episodically flooded endorheic basins (Qa'as) at the edge of the greater Al Jouf oasis region	Ephemeral river systems (wadis)	Pastoral watering, wells, troughs	11.3 ha	Chalcolithic well structures with trough systems; constructed dams to divert or retain surface runoff to increase water exploitation.	Zielhofer et al. (2018)
4	Qurayyah, Saudi Arabia N 28°47′2″ E 36°0′41″ PPNB – late Byzantine period Most significant extent during the Bronze Age	Located in the transitional region between the plateau landscape of the eastern Hejaz and the Tabuk basin, influenced by two cross-regional wadis, Wadi Harif and Wadi Ghubai, on ~800 m a.s.l; in a quasi-planar widening of a side valley branching from Wadi Ghubai with an area of approximately 7.3 km², slightly dipping with ~0.5° on average and intertwined with shallow, playa-like depressions.	Ephemeral river system (wadi) Fracture springs	The water from the fracture spring(s) may have been used for drinking purposes.Water for flood irrigation and pottery production was most likely gathered by surface water harvesting from Wadi Ghubai.	116 ha inside the walls with additional ca. 100 ha outside the walls	SWH structures, including a dam, inlet and outlet breaching the city walls were used. Irrigation canals were used to extend the flooded area.	Hüneburg et al. (2019), Ingraham et al. (1981), Luciani (2016), Luciani and Alsaud (2018), Luciani (2019, 2021a), Parr et al. (1970)
5	Ein Ghedi, Israel N 31°27′17.60″ E 35°22′46.00″ 7th century BCE – 6th century CE	In the west, Ein Ghedi was delimited by a cliff higher than 200 m. At the base of this cliff, a line of springs separates an adjacent eastward inclining slope. Beyond the slope, a plain reaches to the Dead Sea.	Groundwater usage	More than ten, primarily small, active springs supplied the oasis with fresh water.	110 ha	During the Roman-Byzantine period, the cultivated area was at its maximum with 110 ha. Nevertheless, the whole area was not cultivated simultaneously, and some parts were neglected over time. During the Iron Age, the fields were small and only found at the plain below Tell Goren. Two water systems were identified: The first water system protected the agricultural area, diverting floodwater away from it. The second one was a combination of a spring, a reservoir and irrigation canals to transport the water to the terraces.	Hadas (2012)

(Continued)

Table 3. (Continued)

	Location	Geomorphology	Water source	Water usage	Irrigated area	Additional info	References
6	Tayma, Saudi Arabia N 27°37′37″ E 38°32′′60″ Earliest known human presence late 7th/early 6th millennium BCE – until today Oasis cultivation started ~4600 BCE	Several graben systems, including Tayma-graben, a tectonic depression, affect the gentle north-northeast dipping plain on ~830 m a.s.l. Hill ranges surround it.	Groundwater usage Ephemeral river system (wadi) Sabkha	Several wadis fed the sabkha. Wells and springs give access to the groundwater. Water canals were used for irrigation.		The absence of water reservoirs led to the hypothesis that a continuous water supply was available (as is the case nowadays). In the palm garden, several wells were found.	Hamann et al. (2008), Hausleiter and Eichmann (2018), Wellbrock et al. (2018, 2017)
7	Tall Hujayrat al-Ghuzlan, Jordan N 29°34′11″ E 35°1′59″ ~4000–3500 cal BCE	This site is situated on an alluvial terrace, above the wadi bed on ~110 m a.s.l.	Groundwater Usage	The springs were fed by artesian groundwater.	10 ha	The settlement was situated in a hydrologically advantageous location. It was built on elevated terraces to protect it from floods, and springs were close-by. For water collection, retention and distribution, a combination of artesian springs, dams, basins and channels were used. Numerous remains of these surface structures were identified. An individual field measured between 400 and 800 m².	Rhodius et al. (2017), Siegel (2009), Heemeier et al. (2009)
8	Qulban Bani Murra, Jordan N 30°3′1″ E 37°9′13″ Late Chalcolithic- Early Bronze Age	Built on both banks of the Wadi Sahab. Hammada hills flank the wadi.	Groundwater usage Water harvesting	Wells were used to access groundwater. Dams were used for water harvesting. A channel irrigation system was used.		Watering places were positioned on the central wadi floor in the second half of the fifth millennium BCE. Watering or well complexes were split into different spaces. One was excavated, showing a staircase leading to a 'well room' with a 'well mouth', roundish basins.	Al Khasawneh et al. (2016), Gebel and Mahasneh (2013), Gebel (2017), Gebel and Wellbrock (2019)
9	Dumat al-Jandal, Saudi Arabia N 29°48′40.60″ E 39°52′04.51″ 1st millennium BCE – today	The oasis is bordered by a limestone plateau in the north and the Nafud desert in the south. A palaeofloodbed of the Wadi al-Sirhan and a palaeolake or endorheic basin are assumed near the oasis (Late Pleistocene to Mid-Holocene). Today's appearance is a shallow depression (~8 km length, ~3.5 km width).	Groundwater usage Sabkha	Groundwater was accessed with the help of wells. Some wells were equipped with staircases to reach the well's bottom and reach more easily the head of the qanat.		Until now, 20 qanats were identified, all starting from a 'mother well'. They emerge on the surface as springs in the middle of the oasis. Up to now, 18 springs were identified. From these springs, the water flowed onto palm groves positioned farther downslope. From there, the water flowed further to the sabkha. Ancient weather conditions induced the sabkha to slow salinisation. A high number of wells were found at Dumat al-Jandal. Some of them were connected to the qanat system, whereas others were independent of the system.	Wellbrock et al. (2018), Charloux and Loreto (2014), Loreto (2013), Charloux and Loreto (2016), Charloux et al. (2018)
10	Al-Ula, Saudi Arabia N 26°32′30.3″ E 37°58′29.5″ 5th to late 2nd /early 1st century BCE (Precise erection date of the qanats is unknown)	Al-Ula (valley of villages) was the ancient core of a north-south directed valley. The valley is embedded between two ranges of mountains. ~630 m a.s.l.	Groundwater usage Ephemeral river system (wadi)	Qanats and springs give access to groundwater. Surface water was harvested with the help of a dam across Wadi Muʿtadil.		The water in Al-Ula was used for domestic and agricultural needs, as well as for essential rituals. For the latter, they had built water basins with staircases to reach the bottom and canals. The water for irrigation purposes was obtained from both, groundwater and water harvesting. From the dam, water canals distribute the water over a secondary canals network to the agricultural plots. Qanats: with the help of gravity or a calculated slope, underground canals transported water from a water table to the surface at the base of a plateau or mountain.	Marquaire (2019), Yu (2019)

Conclusions

Notwithstanding the onset of a progressively arid climate after 5500–5000 BCE and continuous aridification thereafter, we witness the establishment of a number of mega-sites in the NW fringes of the Arabian deserts (Luciani, 2021b).

With our interdisciplinary investigation of the geomorphology and anthropic hydraulic infrastructure in one of the largest of these sites, the river oasis (Hüneburg et al., 2019) Qurayyah, we precisely assess chronology and functionality of the water exploitation system of this desert settlement in order to understand the fundamental parameters of the site's formation as an urban-sized permanent settlement and its persistence over three millennia.

After a geomorphological assessment of the micro-region and identifying the functional elements of Qurayyah's SWHS, we cross-checked chronological measurements of OSL samples from four key sites of the system (Table 2a) with radiometric data from organic samples (Table 2b) from controlled stratigraphic excavations inside and outside the archaeological site. This allowed us to prove that the earliest SWHS was established in 2900–2600 BCE, that is, in the Early Bronze Age and was the topographic and economic basis for the formation of the settlement in an extended, 300 ha large walled oasis.

To better clarify our understanding of the identified key elements of the SWHS and their hydrological function, we subjected the parameters measured in the field to a plausibility check.

The plausibility check provides the first precise estimate of the water amount necessary to irrigate the agricultural area through flood irrigation and of the water quantities delivered by Wadi Ghubai. The test proved that Qurayyah's catchment area was capable of providing water far beyond the needs of the oasis dwellers during individual rainfall events. Indirectly, establishing the presence of such a potential surplus in water supports our understanding of the function of the diverting dam (Area E) as bulwark protecting the settlement downstream from potential damage caused by flooding.

Finally, the comparison with water exploitation systems developed in other anthropic settlements in comparable arid settings, revealed the uniqueness in breadth (extended size), scope (micro-region) and singularity of geomorphological context (quasi-planar, no accessible underground aquifers) of Qurayyah's SWHS and its anteriority to all systems comparable in volume, structure and functioning.

While a large water storage facility of the Classical period was described as the so-called 'Roman Site' (Parr et al., 1970) and is still visible in the middle of the agricultural expanse, we have not yet identified with certainty Qurayyah's Bronze Age water storage units.

We cannot exclude that one such site may underlay the later 'Roman Site' or that the areas outside the city walls, in proximity of the inlets (e.g. Area J), functioned intermittently as such reservoirs.

Future investigations will include generating a high-resolution digital terrain model (DTM) of the site (in cooperation with Kanazawa University, Japan) and an intensive survey of all hydraulic/irrigation structures within the walled area and perimeter zones of the settlement as well as stratigraphic investigations at selected locations of both anthropic and natural components of Qurayyah's SWHS.

ORCID iDs

Christopher Lüthgens https://orcid.org/0000-0003-3211-6318

Marta Luciani https://orcid.org/0000-0002-3105-2212

Sabrina Prochazka https://orcid.org/0000-0001-7258-5448

Gustav Firla https://orcid.org/0000-0003-4217-6699

Philipp Hoelzmann https://orcid.org/0000-0001-8709-8474

Supplemental material

Supplemental material for this article is available online.

References

Abushandi E (2016) Flash flood simulation for Tabuk City catchment, Saudi Arabia. *Arabian Journal of Geosciences* 9: 188.

Al-Ahmadi M (2009) Hydrogeology of the saq aquifer northwest of Tabuk, northern Saudi Arabia. *Journal of King Abdulaziz University-Earth Sciences* 20(1): 51–66.

Al-Homoud AS, Allison RJ, Sunna BF et al. (1996) A study on geology, geomorphology, hydrology, groundwater, and physical resources of the desertified Badia environment in Jordan towards sustainable development. *Environmental Geology* 27(3): 198–209.

Al Khasawneh S, Murray AS, Gebel HG et al. (2016) First application of OSL dating to a Chalcolithic well structure in Qulbān Banī Murra, Jordan. *Mediterranean Archaeology & Archaeometry* 16(3): 127–134.

Alsharshan AS, Rizk ZA, Nairn AEM et al. (2001) *Hydrogeology of an Arid Region: The Arabian Gulf and Adjoining Areas*. Amsterdam: Elsevier, pp.366 DOI:10.1016/B978-0-444-50225-4.X5000-3

Arz HW, Lamy F and Pätzold J (2006) A pronounced dry event recorded around 4.2 ka in brine sediments from the northern red Sea. *Quaternary Research* 66(3): 432–441.

Bailey RM and Arnold LJ (2006) Statistical modelling of single grain quartz De distributions and an assessment of procedures for estimating burial dose. *Quaternary Science Reviews* 25(19–20): 2475–2502.

Banerjee D, Murray AS, Bøtter-Jensen L et al. (2001) Equivalent dose estimation using a single aliquot of polymineral fine grains. *Radiation Measurements* 33(1): 73–94.

Bar-Matthews M and Ayalon A (2011) Mid-Holocene climate variations revealed by high-resolution speleothem records from Soreq Cave, Israel and their correlation with cultural changes. *The Holocene* 21(1): 163–171.

Barth HK (1976) Saudi-Arabien: Natur, Geschichte, Mensch und Wirtschaft. In: Helmut B (ed.) *Der Naturraum im überblick*. Stuttgart: Ed. Erdmann, pp.23–44.

Barth HK and Schliephake K (1998) Saudi-Arabien: mit einem Anhang Fakten-Zahlen-Übersichten; sowie 29 Übersichten und 107 Tabellen. Klett-Perthes.

Bollrich G (2013) *Technische Hydromechanik 1: Grundlagen*. Berlin: Beuth.

Bøtter-Jensen L, Andersen CE, Duller GAT et al. (2003) Developments in radiation, stimulation and observation facilities in luminescence measurements. *Radiation Measurements* 37(4–5): 535–541.

Bøtter-Jensen L, Bulur E, Duller GAT et al. (2000) Advances in luminescence instrument systems. *Radiation Measurements* 32(5–6): 523–528.

Bøtter-Jensen L, Thomsen KJ and Jain M (2010) Review of optically stimulated luminescence (OSL) instrumental developments for retrospective dosimetry. *Radiation Measurements* 45(3–6): 253–257.

Charloux G, Courbon P, Testa O et al. (2018) Mapping an ancient qanat system in a northern Arabian urbanized oasis. *Water History* 10(1): 31–51.

Charloux G and Loreto R (2014) Dûma 1. 2010 Report of the Saudi-Italian-French Archaeological Project at Dûmat al-Jandal. Saudi Commission for Tourism and Antiquities.

Charloux G and Loreto R (2016) Dûma 2. The 2011 Report of the Saudi–Italian–French Archaeological Project at Dûmat al-Jandal, Saudi Arabia.

Cherkinsky A, Culp RA, Dvoracek DK et al. (2010) Status of the AMS facility at the University of Georgia. *Nuclear Instruments & Methods in Physics Research Section B, Beam Interactions With Materials and Atoms* 268: 867–870.

Dinies M and Hoelzmann P (2020) Enviromental research, in Luciani M and Alsaud A S, Qurayyah 2015. Report on the first season of the joint Saudi Arabian-Austrian Archaeological Project. *Atlal-The Journal of Saudi Arabian Archaeology* 28: 68–72.

Duller G (2015) The analyst software package for luminescence data: Overview and recent improvements. *Ancient TL* 33(1): 35–42.

Engel M, Brückner H, Pint A et al. (2012) The early Holocene humid period in NW Saudi Arabia – Sediments, microfossils and palaeo-hydrological modelling. *Quaternary International* 266: 131–141.

Fujii S (2014) A half-buried cistern at Wadi Abu Tulayha: A key to tracing the pastoral nomadization in the Jafr Basin, Southern Jordan. In: Jamhawi M (ed.) *Jordan's Prehistory: Past and Future Research*. Amman: Department of Antiquities, pp.159–168.

Fujii S and Abe M (2008) PPNB Frontier in Southern Jordan: A Preliminary Report on the Archaeological Surveys and Soundings in the Jafr Basin, 1995-2005. ラーフィダーン= al-Rāfidān.(29).

Fujii S, Adachi T, Endo H et al. (2012) Wādī an-Nuʿayḏiyyah 1: another Neolithic barrage system in the al-Jafr Basin, Southern Jordan. *Annual of the Department of Antiquities of Jordan* 56: 131–156.

Fujii S, Adachi T, Endo H et al. (2013) Excavations at Wadi Nadiya 2 and supplementary investigations of the Jafr Neolithic barrage system. *Annual of the Department of Antiquities of Jordan* 57: 373–398.

Fujii S, Adachi T, Quintero LA et al. (2011) Wādī Ghuwayr 106: a neolithic barrage system in the north-eastern al-Jafr basin. ‫حولية‬ ‫دائرة‬ ‫الكثار‬ ‫العامة‬ 55.

Fujii S, Adachi T, Yamafuji M et al. (2017) A preliminary report on the Neolithic barrage surveys in the eastern Jafr basin, 2013-2014. *Annual of the Department of Antiquities of Jordan* 58: 585–599.

Galbraith RF, Roberts RG, Laslett GM et al. (1999) Optical dating of single and multiple grains of quartz from jinmium rock shelter, northern Australia: Part I, experimental design and statistical models. *Archaeometry* 41(2): 339–364.

Gebel H (2017) The origins of oasis life in NW Arabia. A model based on the Qulban Beni Murra and Rajajil case study regions, and the need of archaeohydrology as a discipline for studying Arabia's past. In: al-Tikriti W and Yule P (eds) *Water and Life in Arabia*, pp. 1–26, Abu Dhabi: Abu Dhabi Tourism and Culture Authority.

Gebel HGK and Mahasneh H (2013) Disappeared by climate change. The Shepherd cultures of Qulban Beni Murra (2nd half of the 5th millennium BC) and their aftermath. *Syria Archéologie, art et histoire* 90: 127–158.

Gebel H and Wellbrock K (2019) Hydraulic cultures and hydrology under climatic change: North Arabian mid-Holocene pastoral and proto-oasis land use. In: Chiotis E (ed.) *Climate Changes in the Holocene: Impacts and Human Adaptation*. Boca Raton: CRC Press, Taylor & Francis Group, pp.247–269.

Goslar T, Czernik J and Goslar E (2004) Low-energy ^{14}C AMS in Poznań Radiocarbon Laboratory, Poland. *Nuclear Instruments & Methods in Physics Research Section B, Beam Interactions With Materials and Atoms* 223–224: 5–11.

Hadas G (2012) Ancient agricultural irrigation systems in the oasis of Ein Gedi, Dead Sea, Israel. *Journal of Arid Environments* 86: 75–81.

Hajdas I (2008) Radiocarbon dating and its applications in Quaternary studies. *E&G Quaternary Science Journal* 57: 2–24.

Hajdas I, Ascough P, Garnett MH et al. (2021) Radiocarbon dating. *Nature Reviews Methods Primers* 1, 62.

Hamann M, Heemeier B, Patzelt A et al. (2008) Wasserwirtschaftliche Anlagen in der historischen Oasenstadt Tayma, Saudi-Arabien. Cura Aquarum in Jordanien. *Schriften der DWhG, pp.*155-175.

Hausleiter A and Eichmann R (2018) The archaeological exploration of the oasis of Tayma. In: Hausleiter A, Eichmann R and Al-Najem M (eds) *Tayma 1 - Archaeological Exploration, Palaeoenviroment, Cultural Contacts*. Oxford: Archaeopress Publishing LTD, pp.2–59.

Heemeier B, Rauen A, Waldhör M et al. (2009) Water management at Tell Hujayrat al-Ghuzlan. In: Khalil LA and Schmidt K (eds) *Prehistoric ʿAqaba I. R*. Rahden/Westf.: Leidorf, pp. 248–271.

Hüneburg L, Hoelzmann P, Knitter D et al. (2019) Living at the wadi – Integrating geomorphology and archaeology at the oasis of Qurayyah (NW Arabia). *Journal of Maps* 15: 215–226.

Huntley DJ and Lamothe M (2001) Ubiquity of anomalous fading in K-feldspars and the measurement and correction for it in optical dating. *Canadian Journal of Earth Sciences* 38(7): 1093–1106.

Ingraham M, Johnson T, Rihani B et al. (1981) Preliminary report on a reconnaissance survey of the Northwestern Province (with a note on a brief survey of the Northern Province). *Atlal – The Journal of Saudi Arabian Archaeology* 5: 59–84.

Kreutzer S, Schmidt C, Fuchs MC et al. (2012) Introducing an R package for luminescence dating analysis. *Ancient TL* 30(1): 1–8.

Kulig G (2005) Erstellung einer Auswertesoftware zur Altersbestimmung mittels Lumineszenzverfahren. Fakultät für Mathematik und Informatik, TU Freiberg.

Laboun AA (2013) Regional tectonic and megadepositional cycles of the Paleozoic of northwestern and central Saudi Arabia. *Arabian Journal of Geosciences* 6: 971–984.

Loreto R (2013) New Neolithic evidence from the al-Jawf region: an outline of the historical development of Dūmat al-Jandal. Proceedings of the Seminar for Arabian Studies. *JSTOR*, 213–224.

Luciani M (2016) Mobility, Contacts and the Definition of Culture(s) in New Archaeology Research in Norttwest Arabia. In: Marta L (ed.) *The Archaeology of North Arabia. Oases and landscapes*. Wien: Verlag der Österreichischen Akademie der Wissenschaften, pp.21–56.

Luciani M (2019) Qurayyah. In: Capodiferro A and Colantonio S (eds) *Roads of Arabia: Archaeological Treasures From Saudi Arabia*. Milano: Mondadori Electa S.p.A, pp.140–155.

Luciani M (2021a) Canons of iconography water animals, gods and humans. In: Bührig C, van Ess M, Gerlach I, et al (eds)

Klänge der Archäologie Festschrift for Ricardo Eichmann. Wiesbaden: Harrassowitz Verlag / The Publishing House, pp.277–288.

Luciani M (2021b) On the formation of 'Urban' oases in Arabia: New Perspectives from the northwest. In: Luciani M (ed.) *The Archaeology of the Arabian Peninsula 2: Connecting the Evidence. OREA 19.* Wien: Verlag der Österreichischen Akademie der Wissenschaften, pp.89–118.

Luciani M and Alsaud AS (2018) The new archaeological joint project on the site of Qurayyah, north-west Arabia: results of the first two excavation seasons. In: *Proceedings of the Seminar for Arabian studies.* Oxford: Archaeopress, pp.165-183.

Lüthgens C, Neuhuber S, Grupe S et al. (2017) Geochronological investigations using a combination of luminescence and cosmogenic nuclide burial dating of drill cores from the Vienna Basin. *Zeitschrift der Deutschen Gesellschaft für Geowissenschaften* 168(1): 115–140.

Lüthgens C, Böse M and Preusser F (2011) Age of the pomeranian ice-marginal position in northeastern Germany determined by optically stimulated luminescence (OSL) dating of glaciofluvial sediments. *Boreas* 40(4): 598–615.

Marquaire C (2019) *Hydraulic Installations. ALULA – WONDER OF ARABIA.* Paris: Institute du monde arabe Editions Gallimard.

Masry AH (1977) The historic legacy of Saudi Arabia. *Atlal-The Journal of Saudi Arabian Archaeology* 1: 9–19.

Mazzoni S (1997) Complex Society, Urbanization and Trade. The Case of Eastern and Western Arabia. In: Avanzini A (ed.) *Profumi d'Arabia.* Rome: Atti del Convegno, pp.23–35.

Meister J, Krause J and Müller-Neuhof B (2018a) Early Bronze Age Jawa – An artificial oasis in the Basalt Desert. In: Berking J and Schütt B (eds) *Water Harvesting in Drylands – Water Knowledge From the Past for Our Present and Future.* München: Verlag Dr. Friedrich Pfeil, pp.40–47.

Meister J, Rettig R and Schütt B (2018b) Ancient runoff agriculture at Early Bronze Age Jawa (Jordan): Water availability, efficiency and food supply capacity. *Journal of Archaeological Science Reports* 22: 359–371.

Meister J, Krause J, Müller-Neuhof B et al. (2017) Desert agricultural systems at EBA Jawa (Jordan): Integrating archaeological and paleoenvironmental records. *Quaternary International* 434: 33–50.

Müller-Neuhof B, Abu-Azizeh L, Abu-Azizeh W et al. (2013) East of Jawa: Chalcolithic/Early Bronze Age settlement activity in al-Ḥarra (north-east Jordan). *Annual of the Department of Antiquities of Jordan* 57: 125–139.

Müller-Neuhof B, Betts A and Wilcox G (2015) Jawa, northeastern Jordan: The first 14C dates for the early occupation phase. *Zeitschrift für Orient-Archäologie* 8: 124–131.

Murray AS and Wintle AG (2000) Luminescence dating of quartz using an improved single-aliquot regenerative-dose protocol. *Radiation Measurements* 32(1): 57–73.

Murray AS and Wintle AG (2003) The single aliquot regenerative dose protocol: potential for improvements in reliability. *Radiation Measurements* 37(4-5): 377–381.

Neugebauer I, Dinies M, Plessen B et al. (2022) The unexpectedly short Holocene humid period in northern Arabia. *Communications Earth & Environment* 3: 47.

Parr PJ, Harding GL and Dayton JE (1970) Preliminary Survey in N.W. Arabia, 1968. *Bulletin of the Institute of Archaeology* 8/9: 193–242.

Preusser F, Degering D, Fuchs M et al. (2008) Luminescence dating: Basics, methods and applications. *E&G Quaternary Science Journal* 57(1/2): 95–149.

Rades EF, Fiebig M and Lüthgens C (2018) Luminescence dating of the Rissian type section in southern Germany as a base for correlation. *Quaternary International* 478: 38–50.

Ramsey CB and Lee S (2013) Recent and planned developments of the program OxCal. *Radiocarbon* 55: 720–730.

Reilly B (2015) *Slavery, Agriculture and Malaria in the Arabian Peninsula.* Athens: Ohio University Press.

Reimer PJ, Austin WEN, Bard E et al. (2020) The IntCal20 Northern Hemisphere radiocarbon age calibration curve (0–55 cal kBP). *Radiocarbon* 62: 725–757.

Rhodes EJ (2011) Optically stimulated luminescence dating of sediments over the past 200,000 years. *Annual Review of Earth and Planetary Sciences* 39: 461–488.

Rhodius C, Kadereit A, Siegel U et al. (2017) Constraining the time of construction of the irrigation system of Tell Hujayrat al-Ghuzlan near Aqaba, Jordan, using high-resolution optically stimulated luminescence (HR-OSL) dating. *Archaeological and Anthropological Sciences* 9(3): 345–370.

Roberts HM (2007) Assessing the effectiveness of the double-SAR protocol in isolating a luminescence signal dominated by quartz. *Radiation Measurements* 42(10): 1627–1636.

Scerri EML, Guagnin M, Groucutt HS et al. (2018) Neolithic pastoralism in marginal environments during the Holocene humid period, northern Saudi Arabia. *Antiquity* 92(365): 1180–1194.

Siegel U (2009) Hydrological Structures in the Wadi al-Yutum Fan in the Vicinity of Tall Hujayrat al-Ghuzlan. In: Khalil LA and Schmidt K (eds) *Prehistoric 'Aqaba I.* Rahden: Verlag Marie Leidorf GmbH, pp.273–294.

Taylor RE and Bar-Yosef O (2014) *Radiocarbon Dating.* New York: Routledge, p.404.

Vincent P (2008) *Saudi Arabia: An Environmental Overview.* London: Taylor & Francis Group.

Wallinga J (2002) On the detection of osl age overestimation using single-aliquot techniques. *Geochronometria: Journal on Methods & Applications of Absolute Chronology* 21: 17–26.

Wellbrock K, Grottker M and Gebel H (2017) Archaeohydrological Investigation in NW Arabia. *Proceedings of Water and Life in Arabia Conference, pp.* 27–44.

Wellbrock K, Voß P, Heemeier B et al. (2018) The Water Management of Tayma and Other Ancient Oasis Settlements in the North-Western Arabian Peninsula – a synthesis. In: Hausleiter A, Eichmann R and Al-Najem M (eds) *Tayma 1 – archaeological exploration, palaeoenviroment, cultural contacts.* Oxford: Archaeopress Publishing LTD, pp.144–200.

Whitney JW, Faulkender D and Rubin M (1983) The environmental history and present condition of Saudi Arabia's northern sand seas. Open-File Report 83-749, United States Department of the Interior – Geological Survey, Denver, Colorado.

Wintle AG (1973) Anomalous fading of thermo-luminescence in mineral samples. *Nature* 245(5421): 143–144.

Wintle AG (2008) Luminescence dating: Where it has been and where it is going. *Boreas* 37(4): 471–482.

Wintle AG and Murray AS (2006) A review of quartz optically stimulated luminescence characteristics and their relevance in single-aliquot regeneration dating protocols. *Radiation Measurements* 41(4): 369–391.

Yu K (2019) Al-Ula Oasis and the Lost Civilization. *Landscape Architecture Frontiers* 7(4): 4–9.

Zielhofer C, Wellbrock K, Al-Souliman AS et al. (2018) Climate forcing and shifts in water management on the Northwest Arabian Peninsula (mid-Holocene Rasif wetlands, Saudi Arabia). *Quaternary International* 473: 120–140.

S1: Detailed description of stratigraphic units shown in Fig. 2				
Area (cf. Fig. 1)	**Coordinates (decimal degrees, WGS 84)**	**Altitude (m)**	**Stratigraphic unit (SU)**	**Description**
G (canal)	28.76191 (N) 36.00279 (E)	794	SU370=SU374	stone slab, canal wall construction
			SU371	silty loam, light beige
			SU372	loose silty loam with bedrock inclusions
			SU373	surface layer, silty loam
			SU 375	like SU372 but with more frequent bedrock scales
E (stone dam)	28.78178 (N) 36.01687 (E)	806	SU 351	brown sand below SU 352
			SU 352	dam construction (unhewn stones and mud mortar)
			SU 353	dark brown loam; natural soil
			SU 354	pinkish-beige sand on SU 351 and under SU 355
			SU 355	pinkish-beige sand on SU 354, more compact than SU 354
J (main inlet)	28.78393 (N) 36.00710 (E)	792	SU 395	bedrock, with manganese spots, yellow
			SU 396	sandy layer, grey/white, with snails embedded
			SU 397	sandy clay, sub clastic, dark grey
			SU 398	sandy loam with small stone inclusions, light grey
			SU 399	silty sand, beige
			SU 400	silty mudbricks, beige
F (outlet)	28.79833 (N) 36.02305 (E)	773	SU 361	sandy bedrock, yellow
			SU 362	sandy loam to fine sand, white carbonate
			SU 363	fine sand, yellow
			SU 364	fine deposits, light beige, possible mudbrick
			SU 365	sandy loam, dark grey

S2: Detailed information on the yardang site (Fig. 1g)

Section Q15-4 (N28°49,262'/E36°02,922') with radiocarbon dates, selected analyses and a short description of the six sampled layers (16 specimen). The section represents playa-like sediment layers that have been deflated to form this yardang. Above mottled sandy layers (layers 6 to 4) with ox-red phenomena, that represent fluctuating levels of ground-water table, a sequence of silty, calcitic to gypsiferous slack water deposits developed (layers 3 to 1). Imbedded molluscs (layer 3) and high percentages of calcite reflect the most stable paleo slack water or even paleolake conditions throughout this section. Increasing gypsum contents towards the top of the yardang point to progressively drier conditions.

EA = elemental analysis; XRD = X-ray diffraction; XRF = portable X-ray fluorescence spectrometry; BCE before common era.

1:
very pale brown (10YR8/2), encrusted silty gypsum layer with single hardened carbonaceous layers.

2:
light grey to grey (10YR7/2 to 10YR6/1) silty gypsum layer; interstratified with organic carbon.

3:
light grey (10YR7/2) to pale yellow (2.5Y8/2), stratified and hardened calcitic layer with imbedded mollusc.

4:
pale yellow (2,5Y8/3) fine sand, bleached.

5:
pale yellow (2.5Y8/2) silty fine sand, hardened by a salty crust.

6:
yellow (10YR8/6), mottled fine sand; partly with thin salt incrustations.